



Search for $B_c^+ \rightarrow \pi^+ \mu^+ \mu^-$ decays and measurement of the branching fraction ratio $\mathcal{B}(B_c^+ \rightarrow \psi(2S)\pi^+)/\mathcal{B}(B_c^+ \rightarrow J/\psi\pi^+)$

LHCb Collaboration

CERN, 1211 Geneva 23, Switzerland

Received: 20 December 2023 / Accepted: 10 March 2024 / Published online: 7 May 2024
© CERN for the benefit of the LHCb collaboration 2024

Abstract The first search for nonresonant $B_c^+ \rightarrow \pi^+ \mu^+ \mu^-$ decays is reported. The analysis uses proton–proton collision data collected with the LHCb detector between 2011 and 2018, corresponding to an integrated luminosity of 9 fb^{-1} . No evidence for an excess of signal events over background is observed and an upper limit is set on the branching fraction ratio $\mathcal{B}(B_c^+ \rightarrow \pi^+ \mu^+ \mu^-)/\mathcal{B}(B_c^+ \rightarrow J/\psi\pi^+) < 2.1 \times 10^{-4}$ at 90% confidence level. Additionally, an updated measurement of the ratio of the $B_c^+ \rightarrow \psi(2S)\pi^+$ and $B_c^+ \rightarrow J/\psi\pi^+$ branching fractions is reported. The ratio $\mathcal{B}(B_c^+ \rightarrow \psi(2S)\pi^+)/\mathcal{B}(B_c^+ \rightarrow J/\psi\pi^+)$ is measured to be $0.254 \pm 0.018 \pm 0.003 \pm 0.005$, where the first uncertainty is statistical, the second systematic, and the third is due to the uncertainties on the branching fractions of the leptonic J/ψ and $\psi(2S)$ decays. This measurement is the most precise to date and is consistent with previous LHCb results.

1 Introduction

The B_c^+ meson is made of the heaviest quarks that bind to form hadrons in the Standard Model (SM): beauty and charm quarks. The presence of two heavy quarks distinguishes the system from other B mesons in theoretical calculations. Hence, measurements of the branching fractions of B_c^+ decay modes can provide unique tests of the understanding of Quantum Chromodynamics.

The B_c^+ meson can decay in various ways as each constituent quark can undergo weak decay with the other as a spectator. The availability of large data samples at the LHC has allowed the observation of the case where the c quark decays [1, 2], complementing a range of observations of transitions to final states mediated by b -quark decays. The B_c^+ meson can also decay through the annihilation of the \bar{b} and c quarks into a virtual W boson, producing either leptonic, semileptonic or hadronic final states. The leptonic final states are challenging to study in a hadron collider environment,

because of the missing energy carried by the neutrino, but are of great interest for investigation at a future high-luminosity e^+e^- collider operating at the Z pole [3–6].

Several B_c^+ decays receiving contributions from annihilation diagrams have been searched for at LHCb, including decays into hadronic final states [7–9] and semileptonic $B_c^+ \rightarrow D_s^+ \mu^+ \mu^-$ decays [10] (the inclusion of charge conjugate processes is implied throughout the paper). However, there has been no previous search for B_c^+ decays to semileptonic final states mediated only by annihilation diagrams, such as nonresonant $B_c^+ \rightarrow \pi^+ \mu^+ \mu^-$ decays. A further interest in these processes is that they may receive contributions from resonant $B_c^+ \rightarrow B_{(s)}^{*0} \pi^+$ decays where the vector $B_{(s)}^{*0}$ state decays via a flavour changing neutral current transition into the $\mu^+ \mu^-$ final state [11]. Such $B_{(s)}^{*0}$ decays are highly suppressed in the SM [12, 13] but could be enhanced in the presence of physics beyond the SM.

In the SM, nonresonant $B_c^+ \rightarrow \pi^+ \mu^+ \mu^-$ decays occur through the annihilation of the \bar{b} and c quarks into a virtual W boson (that decays into the u and \bar{d} quarks that produce the charged pion) with radiation of a virtual photon or Z boson (that decays into a muon pair). Currently, there are no theoretical predictions for this decay mode. Weak annihilation contributions to B^+ decays into the same final state have been investigated as these can result in interesting phenomenology including CP -violation effects [14–18]. It is, however, unclear to what extent the theoretical approaches used in these studies are applicable to B_c^+ decays.

This paper describes the first search for nonresonant $B_c^+ \rightarrow \pi^+ \mu^+ \mu^-$ decays exploiting proton–proton (pp) collision data collected with the LHCb detector, corresponding to an integrated luminosity of 9 fb^{-1} . The analysis strategy is based on the reconstruction of $B_c^+ \rightarrow \pi^+ \mu^+ \mu^-$ candidates, sorted into intervals of the dimuon invariant mass, $m(\mu^+ \mu^-)$, that are expected to be dominated by either nonresonant or resonant contributions. The intervals used are shown in Table 1 (natural units with $\hbar = c = 1$ are used here and throughout the paper). These include regions around the J/ψ and $\psi(2S)$ resonances, where the $B_c^+ \rightarrow J/\psi\pi^+$

^a e-mail: fernando.abudinen@cern.ch (corresponding author)

Table 1 Ranges of dimuon invariant mass or mass squared (q^2) used in the analysis

Decay mode	Interval
$B_c^+ \rightarrow \pi^+ \mu^+ \mu^-$	(low) $0.1 < q^2 < 1.1 \text{ GeV}^2$
	(central) $1.1 < q^2 < 8.0 \text{ GeV}^2$
	(intermediate) $11.0 < q^2 < 12.5 \text{ GeV}^2$
	(high) $15.0 < q^2 < 35.0 \text{ GeV}^2$
$B_c^+ \rightarrow J/\psi \pi^+$	$ m(\mu^+ \mu^-) - m_{J/\psi} < 50 \text{ MeV}$
$B_c^+ \rightarrow \psi(2S) \pi^+$	$ m(\mu^+ \mu^-) - m_{\psi(2S)} < 50 \text{ MeV}$

decay mode is used as a control and normalisation channel and both the J/ψ and $\psi(2S)$ resonances are reconstructed in $\mu^+ \mu^-$ final states. The presence of $B_c^+ \rightarrow \psi(2S) \pi^+$ decays into the same final state allows an updated measurement of the ratio

$$R_{\psi(2S)/J/\psi} \equiv \frac{\mathcal{B}(B_c^+ \rightarrow \psi(2S) \pi^+)}{\mathcal{B}(B_c^+ \rightarrow J/\psi \pi^+)},$$

which has previously been measured at LHCb with smaller data samples [19,20]. The $m(\mu^+ \mu^-)$ intervals to select resonant decays correspond to about ± 4 times the dimuon invariant-mass resolution centred on the known resonance mass [21]. The intervals for the nonresonant $B_c^+ \rightarrow \pi^+ \mu^+ \mu^-$ decay mode are defined in terms of the dimuon mass squared, q^2 , and include two intervals (low and central) below the J/ψ resonance, one (intermediate) between the J/ψ and the $\psi(2S)$ resonances, and one (high) above the $\psi(2S)$ resonance. The latter lies above the production threshold for two charmed hadrons and will receive contributions from broad charmonium resonances.

For each of the intervals, a fit is performed using the B_c^+ candidate invariant mass, $m(\pi^+ \mu^+ \mu^-)$, as discriminating observable. The yield, relative to that for the $B_c^+ \rightarrow J/\psi \pi^+$ normalisation mode, is converted to a result on the relative branching fraction of the given q^2 bin,

$$R_{\pi^+ \mu^+ \mu^- / J/\psi \pi^+} \equiv \frac{\mathcal{B}(B_c^+ \rightarrow \pi^+ \mu^+ \mu^-)}{\mathcal{B}(B_c^+ \rightarrow J/\psi \pi^+)} = \frac{N_{\pi^+ \mu^+ \mu^-}}{N_{J/\psi \pi^+}} \cdot \frac{\varepsilon_{J/\psi \pi^+}}{\varepsilon_{\pi^+ \mu^+ \mu^-}} \cdot \mathcal{B}(J/\psi \rightarrow \mu^+ \mu^-), \quad (1)$$

where N indicates a yield, ε indicates the efficiency determined from simulation with data-driven corrections, and $\mathcal{B}(J/\psi \rightarrow \mu^+ \mu^-)$ is the known branching fraction of the $J/\psi \rightarrow \mu^+ \mu^-$ decay [21]. Here, $\mathcal{B}(B_c^+ \rightarrow \pi^+ \mu^+ \mu^-)$ indicates the $B_c^+ \rightarrow \pi^+ \mu^+ \mu^-$ differential branching fraction integrated over the q^2 range relevant for the given bin.

2 Detector and simulation

The LHCb detector [22,23] is a single-arm forward spectrometer covering the pseudorapidity range $2 < \eta < 5$, designed for the study of particles containing b or c quarks. The detector includes a high-precision tracking system consisting of a silicon-strip vertex detector surrounding the pp interaction region [24], a large-area silicon-strip detector located upstream of a dipole magnet with a bending power of about 4 T m, and three stations of silicon-strip detectors and straw drift tubes [25,26] placed downstream of the magnet. The tracking system provides a measurement of the momentum, p , of charged particles with a relative uncertainty that varies from 0.5% at low momentum to 1.0% at 200 GeV. The minimum distance of a track to a primary pp collision vertex (PV), the impact parameter (IP), is measured with a resolution of $(15 + 29/p_T) \mu\text{m}$, where p_T is the component of the momentum transverse to the beam, in GeV. Different types of charged hadrons are distinguished using information from two ring-imaging Cherenkov detectors [27]. Photons, electrons and hadrons are identified by a calorimeter system consisting of scintillating-pad and preshower detectors, an electromagnetic and a hadronic calorimeter. Muons are identified by a system composed of alternating layers of iron and multiwire proportional chambers [28]. The online event selection is performed by a trigger [29,30], which consists of a hardware stage, based on information from the calorimeter and muon systems, followed by a two-level software stage, which reconstructs the full event.

Simulation is used to optimise the event selection procedure, to model the shape of the B_c^+ candidate invariant-mass distributions and to estimate efficiencies accounting for the effects of the detector acceptance, reconstruction and selection criteria. In the simulation, pp collisions are generated using PYTHIA [31] with a specific LHCb configuration [32]. The production of B_c^+ mesons is simulated using the dedicated generator BcVegPy [33]. Decays of unstable particles are described by EVTGEN [34], in which final-state radiation is generated using PHOTOS [35]. The interaction of the generated particles with the detector, and its response, are implemented using the GEANT4 toolkit [36,37] as described in Ref. [38]. The underlying pp interaction is reused multiple times, with an independently generated signal decay for each [39].

The B_c^+ candidates reconstructed in simulation are weighted to correct for discrepancies between data and simulation associated with the particle-identification [40], track-reconstruction [41] and hardware trigger [42] efficiencies. The simulation is also corrected such that the B_c^+ lifetime corresponds to the current experimental value [21,43,44]. Additional corrections are applied to account for discrepancies in B_c^+ production kinematics, event track multiplicity and other observables used in the selection of B_c^+ candi-

dates. These corrections are obtained using a multivariate algorithm [45], which is trained using $B_c^+ \rightarrow J/\psi \pi^+$ decays in background-subtracted data and simulation. After the corrections are applied, the simulated distributions of all variables used in the analysis are in good agreement with the data.

3 Candidate selection and background sources

Candidate $B_c^+ \rightarrow \pi^+ \mu^+ \mu^-$ decays are triggered in an identical manner as described in Ref. [46] for B^+ decays to the same final states. The hardware stage of the trigger selects events containing at least one muon with high p_T . The software stage of the trigger selects events containing at least one high- p_T muon that is inconsistent with originating from any PV. The events must contain at least one secondary vertex (formed by two or more of the final-state particles) that is significantly displaced from every PV. A multivariate algorithm [47, 48] is used to identify secondary vertices consistent with the decay of a b hadron.

The initial stages of the offline selection are also similar to those for $B^+ \rightarrow \pi^+ \mu^+ \mu^-$ decays [46], except that less stringent impact parameter and flight distance requirements are imposed to account for the shorter B_c^+ lifetime compared to that of the B^+ meson. The B_c^+ candidates are formed from pairs of well-reconstructed oppositely charged tracks that are identified as muons together with a track identified as a pion, and are required to have a good-quality vertex. Each B_c^+ candidate is associated with the PV giving the smallest value of χ_{IP}^2 , which is defined as the difference in the vertex-fit χ^2 of the PV reconstructed with and without the candidate. Each B_c^+ candidate must be consistent with originating from its associated PV, and have a momentum vector aligned with the direction between the primary and B_c^+ decay vertices.

Each B_c^+ candidate is required to have an invariant mass in the range $6150 < m(\pi^+ \mu^+ \mu^-) < 6700$ MeV. The expected signal resolution in $m(\pi^+ \mu^+ \mu^-)$ corresponds to about 20 MeV. For the resonant $B_c^+ \rightarrow J/\psi \pi^+$ ($B_c^+ \rightarrow \psi(2S) \pi^+$) decay mode, the B_c^+ candidate mass is calculated from a kinematic fit in which the invariant mass of the J/ψ ($\psi(2S)$) candidate is constrained to the known J/ψ ($\psi(2S)$) mass [21], thereby improving the signal resolution by a factor of about two.

Combinatorial background arising from random combinations of tracks is suppressed using a multivariate classifier. A boosted decision tree (BDT) algorithm [49], as implemented in the XGBoost library [50], is trained to identify the $B_c^+ \rightarrow \pi^+ \mu^+ \mu^-$ signal candidates irrespective of dimuon invariant mass. The signal sample used for the training comprises simulated nonresonant $B_c^+ \rightarrow \pi^+ \mu^+ \mu^-$ decays, resonant $B_c^+ \rightarrow J/\psi \pi^+$ decays, and $B_c^+ \rightarrow B^{*0}(\mu^+ \mu^-) \pi^+$ and $B_c^+ \rightarrow B_s^{*0}(\mu^+ \mu^-) \pi^+$ decays. The latter two popu-

late the high q^2 region, which is sparsely populated in the nonresonant $B_c^+ \rightarrow \pi^+ \mu^+ \mu^-$ simulation. The background training sample comprises data from low- and high-mass sideband regions corresponding to $5550 < m(\pi^+ \mu^+ \mu^-) < 5850$ MeV and $6700 < m(\pi^+ \mu^+ \mu^-) < 7000$ MeV, with vetoes to remove candidates containing $J/\psi \rightarrow \mu^+ \mu^-$ and $\psi(2S) \rightarrow \mu^+ \mu^-$ decays. The features of the data used to classify B_c^+ candidates are: the p_T of the pion track; the p_T of the muon track with highest p_T ; the IPs of the muon tracks and the B_c^+ candidate, the B_c^+ flight distance, the vertex quality of the B_c^+ candidate; and the largest distance of closest approach between any two of the final-state particles.

Requirements on the BDT output and variables characterising the charged pion particle identification are optimised simultaneously using a grid search to obtain the best signal sensitivity. The requirements are optimised independently for the search for the nonresonant $B_c^+ \rightarrow \pi^+ \mu^+ \mu^-$ decays and for the measurement of $R_{\psi(2S)/J/\psi}$. For the search for the $B_c^+ \rightarrow \pi^+ \mu^+ \mu^-$ decay, the optimisation is based on the figure of merit $\varepsilon/(5/2 + \sqrt{N_B})$ [51], where ε is the efficiency on the combined signal sample and N_B is the expected number of background candidates in the signal region (corresponding to an interval of about ± 3 times the B_c^+ invariant-mass resolution centred on the known B_c^+ mass [21]). The expected background yield is estimated by fitting a background-only model to the dataset excluding the signal region. For the measurement of $R_{\psi(2S)/J/\psi}$, the optimisation is based on the figure of merit $N_S/\sqrt{N_S + N_B}$, where N_S and N_B correspond to the expected number of signal and background events in the signal region for the $B_c^+ \rightarrow \psi(2S) \pi^+$ decay. The expectation for N_S is calculated from the signal efficiency and the $B_c^+ \rightarrow \psi(2S) \pi^+$ decay yield from a fit to the data with only a loose requirement on the BDT output applied. The fit model is described below.

The optimal requirements for the nonresonant $B_c^+ \rightarrow \pi^+ \mu^+ \mu^-$ search and for the $R_{\psi(2S)/J/\psi}$ measurement are referred to subsequently as the $\pi^+ \mu^+ \mu^-$ and the $\psi(2S) \pi^+$ working points (WPs), respectively. At the $\pi^+ \mu^+ \mu^-$ WP, the classifier has a combinatorial background rejection power of 99.9%, whilst retaining 27.1% of signal decays. At the $\psi(2S) \pi^+$ WP, the classifier has a combinatorial background rejection power of 98.8%, whilst retaining 63.3% of signal decays. In both cases, the particle identification requirements have a pion efficiency around 90%, with a kaon misidentification rate around 10%. The particle identification requirements applied on the muon candidates have an efficiency around 99%, with a pion misidentification rate below 1%. To measure branching fraction ratios, the same selection is used for the signal and for the normalisation modes, such that potential systematic biases on the measurement are reduced. For both WPs, each selected event contains only one retained candidate.

Backgrounds from partially reconstructed decays such as $B_c^+ \rightarrow \rho^+ \mu^+ \mu^-$ (with ρ^+ decaying into $\pi^+ \pi^0$) for the nonresonant signal mode, $B_c^+ \rightarrow J/\psi \rho^+$ for the normalisation mode, or $B_c^+ \rightarrow \psi(2S) \rho^+$ for the signal $B_c^+ \rightarrow \psi(2S) \pi^+$ mode, have a reconstructed B_c^+ candidate invariant mass that lies more than 100 MeV below the known B_c^+ mass [21]. These sources of background predominantly populate a region outside, but have a tail that extends into, the fit range used in the analysis. This contribution is neglected in the fits to the nonresonant $B_c^+ \rightarrow \pi^+ \mu^+ \mu^-$ candidates, but is accounted for in the resonant mode fits. Backgrounds with a missing neutrino or two or more missing massive particles can also be a source of partially reconstructed background, but their contributions are negligible in the fit range.

Due to the imperfect pion-kaon separation, misidentified backgrounds can in principle arise from $B_c^+ \rightarrow K^+ \mu^+ \mu^-$ decays for the nonresonant signal mode, $B_c^+ \rightarrow J/\psi K^+$ for the $B_c^+ \rightarrow J/\psi \pi^+$ mode, or $B_c^+ \rightarrow \psi(2S) K^+$ for the $B_c^+ \rightarrow \psi(2S) \pi^+$ mode. However, the branching fractions for these sources of background are Cabibbo-suppressed with respect to the signal decays. For instance, the ratio of the $B_c^+ \rightarrow J/\psi K^+$ and $B_c^+ \rightarrow J/\psi \pi^+$ branching fractions has been measured to be $0.079 \pm 0.007 \pm 0.003$ [52]. These background contributions are further suppressed by the particle identification requirements. Due to its estimated size, the Cabibbo-suppressed background is neglected for the search for $B_c^+ \rightarrow \pi^+ \mu^+ \mu^-$ decays. The corresponding background sources are, however, included in the resonant signal mode fits.

Contributions from hadronic backgrounds such as $B_c^+ \rightarrow \pi^+ \pi^- \pi^+$ decays, where two pions are mistakenly identified as muons are expected to be negligible based on the misidentification rates estimated from simulation and the fact that these decays – which have not yet been observed – are expected to occur via suppressed annihilation processes. For the search for the nonresonant $B_c^+ \rightarrow \pi^+ \mu^+ \mu^-$ decay, it is in principle possible to receive contributions from the resonant $B_c^+ \rightarrow J/\psi \pi^+$ or $B_c^+ \rightarrow \psi(2S) \pi^+$ decays, where the π^+ is mistakenly identified as a μ^+ and vice versa. These sources of background are studied using simulation and data and found to be negligible after applying the selection requirements.

4 Invariant-mass fits

The yields for nonresonant $B_c^+ \rightarrow \pi^+ \mu^+ \mu^-$ decays, resonant $B_c^+ \rightarrow J/\psi \pi^+$ decays, and resonant $B_c^+ \rightarrow \psi(2S) \pi^+$ decays are determined from one-dimensional extended unbinned maximum-likelihood fits to the $m(\pi^+ \mu^+ \mu^-)$ distribution of the selected candidates in the respective dimuon invariant-mass intervals (see Table 1). For the resonant decays, the fits are performed independently to the B_c^+ candidates fulfilling the $\pi^+ \mu^+ \mu^-$ WP requirements

and for B_c^+ candidates fulfilling the $\psi(2S) \pi^+$ WP requirements (see Sect. 3). The fits at the $\pi^+ \mu^+ \mu^-$ WP are performed to the $\pi^+ \mu^+ \mu^-$ invariant-mass distribution without additional constraints. The fits at the $\psi(2S) \pi^+$ WP are performed to the B_c^+ candidate mass distribution after constraining the dimuon mass to the known J/ψ or $\psi(2S)$ mass [21], as appropriate.

For the search for the nonresonant $B_c^+ \rightarrow \pi^+ \mu^+ \mu^-$ decay, fits are performed independently for each of the four q^2 intervals and for the combination of the four intervals. The fit model includes two components: signal decays and combinatorial background. The signal model is validated using simulation and corresponds to the sum of two Gaussian functions, one with power-law tails on both sides of the distribution [53]. The tail parameters are fixed to the values obtained from simulation. The signal model includes a global shift of peak position and a global scaling factor for the width of the distribution, relative to the values found in simulation. The peak offset and width scale factor are obtained from a fit to the resonant $B_c^+ \rightarrow J/\psi \pi^+$ decays in data. The combinatorial background is described by an exponential function, whose exponent is allowed to vary in the fit to data.

Figure 1 shows the B_c^+ candidate invariant-mass distributions of selected $B_c^+ \rightarrow \pi^+ \mu^+ \mu^-$ candidates, with results of the fits superimposed. For the intermediate q^2 interval, the fit favours a negative signal yield due to a lack of candidates in the region close to the B_c^+ mass peak position and a feature of extended maximum-likelihood fits that prefers negative yields in such situations [54]. Table 2 summarises the yields obtained from the fits.

For the resonant $B_c^+ \rightarrow J/\psi \pi^+$ decay, the fit model includes four components: signal $B_c^+ \rightarrow J/\psi \pi^+$ decays, misidentified $B_c^+ \rightarrow J/\psi K^+$ decays, partially reconstructed background from $B_c^+ \rightarrow J/\psi \rho^+$ decays and combinatorial background. The signal, misidentified and partially reconstructed backgrounds are each parameterised by the sum of two Gaussian functions, one with power-law tails. The tail parameters of each distribution are fixed from simulation. The peak position and width of the distributions are allowed to vary in the fit to the data by a global offset and scale factor that is shared between the components. The combinatorial background model is an exponential function, whose exponent is allowed to vary in the fit to data. In total, the $B_c^+ \rightarrow J/\psi \pi^+$ fit includes seven free parameters: the yields of the four components, the global peak position shift and width scaling factor, and the exponent of the combinatorial background.

Figure 2 shows the distributions of selected $B_c^+ \rightarrow J/\psi \pi^+$ candidates for both WPs, with fit projections overlaid. Table 3 summarises the yields obtained from the fits. The ratio of $B_c^+ \rightarrow J/\psi \pi^+$ yields at the two WPs is found to be consistent with the expectation based on the efficiencies in simulation. The yields of the misidentified $B_c^+ \rightarrow J/\psi K^+$ com-

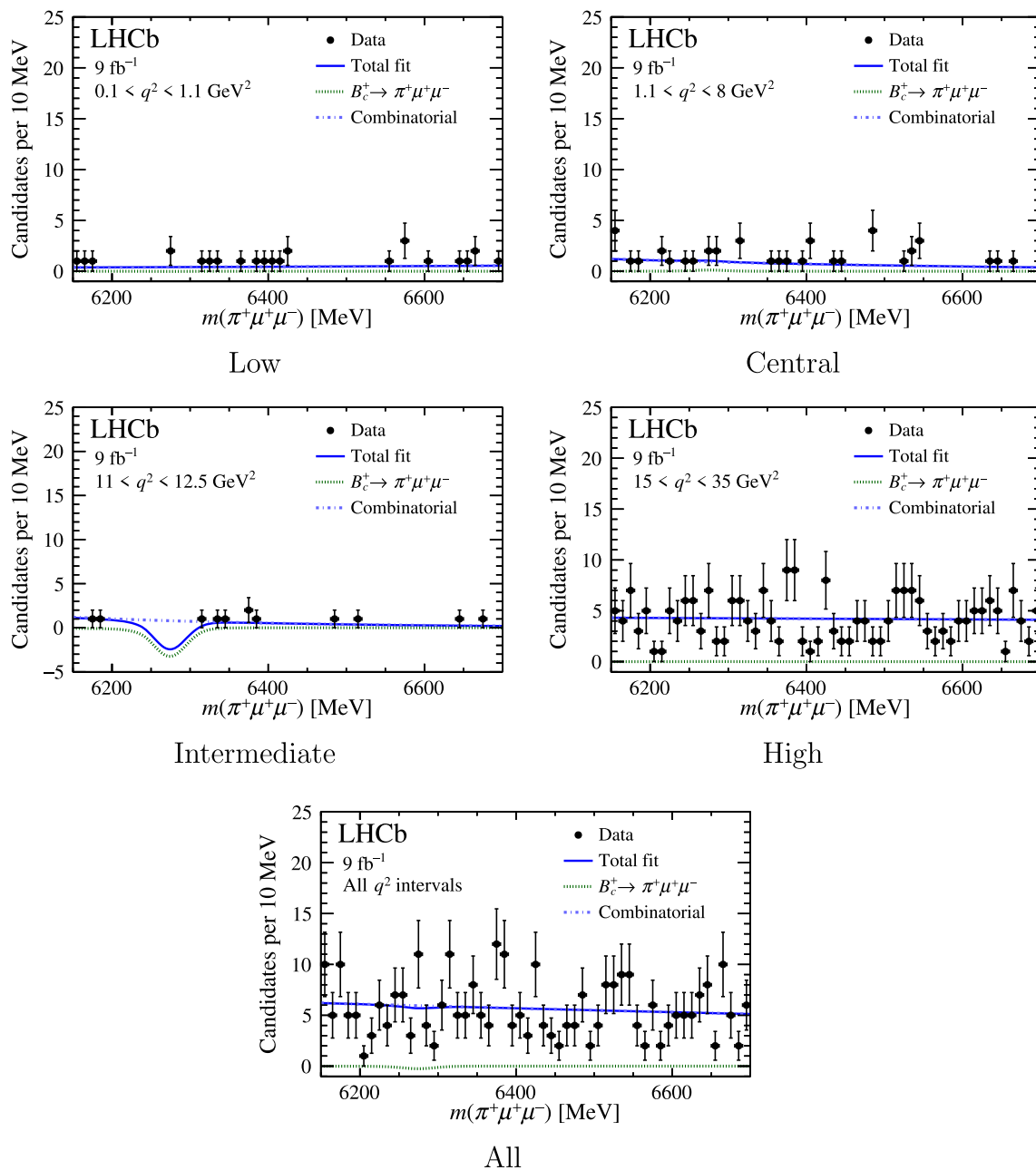


Fig. 1 Reconstructed $\pi^+\mu^+\mu^-$ invariant-mass distributions for the selected $B_c^+ \rightarrow \pi^+\mu^+\mu^-$ candidates for each q^2 interval and for all intervals combined, with results of the fit described in the text overlaid

Table 2 Yields for the signal nonresonant $B_c^+ \rightarrow \pi^+\mu^+\mu^-$ decay ($N_{\pi^+\mu^+\mu^-}$) and combinatorial background (N_{comb}) obtained from the fits to data described in the text, with statistical uncertainties only

q^2 interval	$N_{\pi^+\mu^+\mu^-}$	N_{comb}
$0.1 < q^2 < 1.1 \text{ GeV}^2$	0 ± 2	25^{+6}_{-5}
$1.1 < q^2 < 8.0 \text{ GeV}^2$	1^{+4}_{-3}	39 ± 7
$11.0 < q^2 < 12.5 \text{ GeV}^2$	-18^{+7}_{-10}	30^{+13}_{-9}
$15.0 < q^2 < 35.0 \text{ GeV}^2$	0^{+8}_{-7}	232 ± 17
All	-2^{+9}_{-8}	311^{+20}_{-19}

ponent at the two WPs are found to be consistent with the expectations based on the misidentification rates in simulation and the measured ratio of branching fractions $\mathcal{B}(B_c^+ \rightarrow J/\psi K^+)/\mathcal{B}(B_c^+ \rightarrow J/\psi \pi^+)$ [52].

Similarly, for the resonant $B_c^+ \rightarrow \psi(2S)\pi^+$ decay, the fit includes four components: signal $B_c^+ \rightarrow \psi(2S)\pi^+$ decays, misidentified background from $B_c^+ \rightarrow \psi(2S)K^+$ decays, partially reconstructed $B_c^+ \rightarrow \psi(2S)\rho^+$ background and combinatorial background. The analytical functions of the fit models used for the $B_c^+ \rightarrow \psi(2S)\pi^+$ fit are the same as

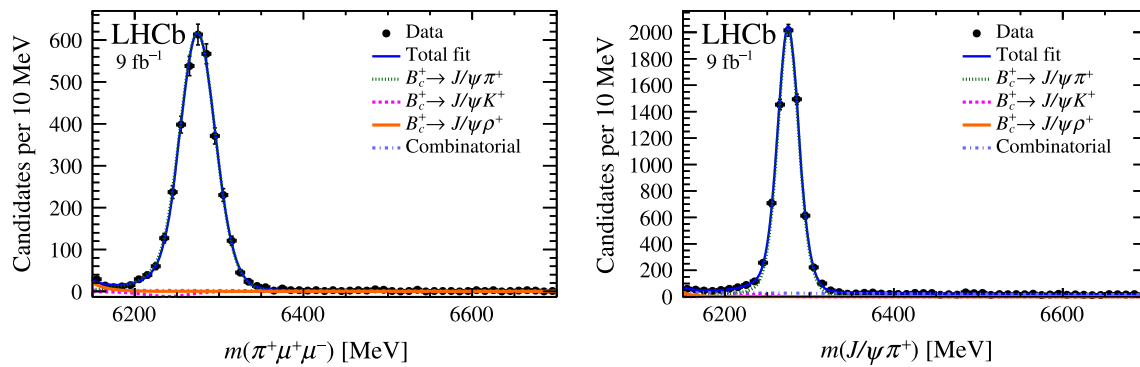


Fig. 2 Reconstructed $\pi^+\mu^+\mu^-$ invariant-mass distributions for the selected $B_c^+ \rightarrow J/\psi\pi^+$ candidates at the (left) $\pi^+\mu^+\mu^-$ and (right) $\psi(2S)\pi^+$ working points, with the results of the fits overlaid. For the

right figure, the $\pi^+\mu^+\mu^-$ invariant mass is calculated after constraining the dimuon mass to the known J/ψ mass, thereby improving the signal resolution

those used for the $B_c^+ \rightarrow J/\psi\pi^+$ fit, but with different parameters. The signal model, and the models for the misidentified and the partially reconstructed background have tail parameters which are fixed to values obtained from simulation, and they also include a global shift of peak position and a global scaling factor for the widths of the distributions. However, the global peak position shift and width scaling factor are constrained in the fit to data to be consistent with the values obtained from the $B_c^+ \rightarrow J/\psi\pi^+$ fit. Thus, the $B_c^+ \rightarrow \psi(2S)\pi^+$ fit includes five free parameters: the yields for the four components and the exponent of the combinatorial background. The $B_c^+ \rightarrow \psi(2S)\pi^+$ fit is performed to the B_c^+ mass distribution after constraining the dimuon mass to the known $\psi(2S)$ mass. Figure 3 shows the distribution of selected $B_c^+ \rightarrow \psi(2S)\pi^+$ candidates, with fit projections overlaid. Table 4 summarises the yields obtained from the fit.

Table 3 Yields obtained from the $B_c^+ \rightarrow J/\psi\pi^+$ fits to data at the two working points as described in the text, with statistical uncertainties only

Component	$\pi^+\mu^+\mu^-$ WP	$\psi(2S)\pi^+$ WP
$B_c^+ \rightarrow J/\psi\pi^+$	3508 ± 82	6887 ± 93
$B_c^+ \rightarrow J/\psi K^+$	-81 ± 58	90 ± 43
$B_c^+ \rightarrow J/\psi\rho^+$	41 ± 11	56 ± 22
Comb. bkg.	101 ± 25	1254 ± 60

5 Efficiencies and systematic uncertainties

The efficiency ratios between signal and normalisation modes are obtained from simulation accounting for the geometrical acceptance of the detector as well as effects related to the triggering, reconstruction and selection of the B_c^+ candidates. Table 5 lists the efficiency ratios between signal and normalisation modes. For the nonresonant signal mode, the efficiency denominator includes only the generated events in the respective q^2 interval. The uncertainties on the efficiency ratios take into account the simulation sample size, uncertainties on the weights applied to the simulation, the matching between reconstructed and generated particles in the simulation, variations of the software trigger requirements, and the uncertainty on the known B_c^+ lifetime. All variations are made consistently for the signal and normalisation modes to avoid overestimation of the uncertainty on the efficiency ratio. For the nonresonant signal mode, the impact of the sig-

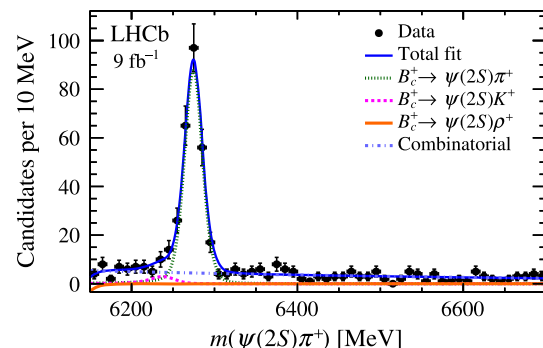


Fig. 3 Reconstructed $\pi^+\mu^+\mu^-$ invariant-mass distribution, calculated after constraining the dimuon mass to the known $\psi(2S)$ mass, for the selected $B_c^+ \rightarrow \psi(2S)\pi^+$ candidates, with results of the fit described in the text overlaid

nal decay model assumed in the simulation is additionally considered.

The systematic uncertainties associated with the weights are evaluated by varying all weights within their uncertainties and by varying the binning scheme used to estimate them. The systematic uncertainty associated with the multivariate weighting algorithm (see Sect. 2) is evaluated by comparing the results obtained with the default and with an alternative algorithm. The default algorithm is trained to correct for discrepancies between data and simulation associated with the

Table 4 Yields obtained from the $B_c^+ \rightarrow \psi(2S)\pi^+$ fit to data described in the text, with statistical uncertainties only

Component	Yield
$B_c^+ \rightarrow \psi(2S)\pi^+$	256 ± 18
$B_c^+ \rightarrow \psi(2S)K^+$	13 ± 10
$B_c^+ \rightarrow \psi(2S)\rho^+$	-4 ± 5
Comb. bkg.	197 ± 19

Table 5 Efficiency ratios between signal and normalisation modes. The values of $\varepsilon_{J/\psi\pi^+}/\varepsilon_{\pi^+\mu^+\mu^-}$ are provided for each q^2 interval and for all intervals combined. The uncertainty on the ratio combines statistical and systematic effects

Signal decay mode		$\varepsilon_{J/\psi\pi^+}/\varepsilon_{\pi^+\mu^+\mu^-}$
$B_c^+ \rightarrow \pi^+\mu^+\mu^-$	(low)	1.26 ± 0.24
	(central)	1.27 ± 0.18
	(intermediate)	0.91 ± 0.04
	(high)	0.86 ± 0.24
	(all)	1.01 ± 0.27
$B_c^+ \rightarrow \psi(2S)\pi^+$		0.91 ± 0.01

event track multiplicity and with the p_T and the vertex quality of the B_c^+ candidates. The alternative algorithm is trained using the IPs of the two muons as additional inputs.

The systematic uncertainty associated with the matching between reconstructed and generated particles in the simulation is evaluated by comparing the efficiencies obtained including or excluding B candidates for which one or more decay products are not correctly matched. The systematic uncertainty associated with variations of the software trigger requirements that are not mirrored by the simulation is evaluated by comparing the efficiencies obtained by applying the tightest thresholds and by applying average thresholds within each data-taking period. The systematic uncertainty associated with the B_c^+ lifetime is evaluated by varying the B_c^+ lifetime in simulation within its uncertainties [21].

The nonresonant signal decays are simulated with a phase-space distribution of the final-state particles. However, the true q^2 distribution of $B_c^+ \rightarrow \pi^+\mu^+\mu^-$ decays is unknown, and there is no clear theoretical guidance for its expectation. A systematic uncertainty is assigned due to the change of efficiency over q^2 , shown in Fig. 4. The uncertainty is taken to be the root-mean-square variation of the distribution of the efficiency values in narrow q^2 bins within each interval. The approach of determining the differential branching fraction within q^2 bins helps to reduce this uncertainty.

A similar uncertainty arises due to the different possible polarisations in the dimuon system, and is illustrated by the different coloured distributions in Fig. 4. The two extreme possibilities correspond to the dimuon system forming a scalar state, which is unpolarised, and a vector state that

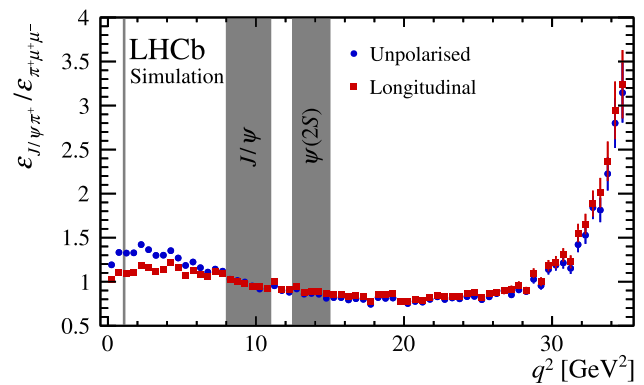


Fig. 4 Efficiency ratio between the $B_c^+ \rightarrow J/\psi\pi^+$ and nonresonant $B_c^+ \rightarrow \pi^+\mu^+\mu^-$ decay modes as a function of q^2 , evaluated for the two extreme possibilities of the dimuon system forming a scalar state, which is unpolarised, and a vector state that is longitudinally polarised. The shaded q^2 intervals, which contain the contributions from the J/ψ and $\psi(2S)$ resonances, are not used in the analysis of nonresonant decays

is longitudinally polarised. The two cases are characterised by different $\cos\theta_l$ distributions, where the helicity angle θ_l is defined as the angle between the μ^+ momentum and the opposite of the B^+ momentum in the dimuon frame: the scalar dimuon state corresponds to a flat $\cos\theta_l$ distribution, while the vector dimuon state corresponds to a $\frac{3}{4}\sin^2\theta_l$ distribution. The difference in efficiency between the two extreme cases is taken as the associated systematic uncertainty.

For the resonant modes, the effect of the multivariate weighting algorithm dominates the systematic uncertainty on the efficiency ratio, while for the nonresonant signal mode, the systematic uncertainty associated with efficiency variation within the q^2 intervals dominates the uncertainty on the efficiency ratio. The remaining systematic uncertainties cancel out almost fully in the determination of the efficiency ratios. For all measured quantities, the systematic uncertainties are smaller than the statistical uncertainties.

The yields obtained from the fits described in the previous section can be affected by the fit model choice and by the assumption of the polarisation of the partially reconstructed backgrounds. To study the effect of the fit model choice, each fit is performed in two configurations: using the baseline fit model and using an alternative fit model. In the alternative fit model, the analytical function used for the signal and the misidentified background models is replaced with the sum of two Gaussian functions, one with a power-law tail on the left side of the distribution, and the other with a power-law tail on the right. The analytical function for the partially reconstructed backgrounds is also replaced, but with the sum of two Gaussian functions. In all cases the difference between the results obtained with the baseline and alternative models is found to be negligible.

For the fits to nonresonant signal candidates, the possible contribution from partially reconstructed $B_c^+ \rightarrow \rho^+\mu^+\mu^-$

decays is found to be negligible by performing fits to sideband data of background-only models including a $B_c^+ \rightarrow \rho^+ \mu^+ \mu^-$ background component. The sideband data includes B_c^+ candidates in the fit range excluding those in the signal region (see Sect. 3). For the resonant modes, the ρ^+ meson is assumed to be unpolarised. However, the polarisation of the ρ^+ meson can affect the momentum of the missing pion and hence the B_c^+ candidate mass shape of the partially reconstructed backgrounds. To study the effect of the ρ^+ polarisation, the fits are repeated assuming either full longitudinal or full transverse ρ^+ polarisation. The difference in the results for the two configurations is found to be negligible.

6 Results

For the nonresonant signal mode, no signal is observed over the background-only hypothesis and an upper limit is set on $R_{\pi^+ \mu^+ \mu^- / J/\psi \pi^+}$ in each q^2 bin. The ratio $R_{\pi^+ \mu^+ \mu^- / J/\psi \pi^+}$ is obtained by parametrising the signal yield $N_{\pi^+ \mu^+ \mu^-}$ in the fits described in Sect. 4 using Eq. (1). The branching fraction $\mathcal{B}(J/\psi \rightarrow \mu^+ \mu^-)$ [21], the efficiency ratio $\varepsilon_{J/\psi \pi^+} / \varepsilon_{\pi^+ \mu^+ \mu^-}$, and the normalisation yield $N_{J/\psi \pi^+}$ are allowed to vary within Gaussian constraints to account for the uncertainties on these inputs.

Upper limits on the branching fraction ratios are obtained following the Feldmann–Cousins prescription [55]: pseudo-experiments are generated for various values of $R_{\pi^+ \mu^+ \mu^- / J/\psi \pi^+}$ and the resulting distribution of measured $R_{\pi^+ \mu^+ \mu^- / J/\psi \pi^+}$ is used to form confidence belts. Figure 5 shows confidence belts at 90% and 95% confidence level (CL). Table 6 gives the results for $R_{\pi^+ \mu^+ \mu^- / J/\psi \pi^+}$ and the obtained limits. To assess the impact of the systematic uncertainties, the fits are repeated fixing the nuisance parameters to their central values. Figure 6 summarises the obtained limits on the normalised differential branching fraction. As further checks the procedure is repeated restricting the signal yield to positive values, or performing nonextended maximum-likelihood fits. No significant changes in the obtained upper limits are found.

For the resonant modes, the yields obtained from the fits and the efficiency ratio are used to calculate the fraction

$$F_{\psi(2S)/J/\psi} = \frac{N_{\psi(2S)\pi^+}}{N_{J/\psi\pi^+}} \cdot \frac{\varepsilon_{J/\psi\pi^+}}{\varepsilon_{\psi(2S)\pi^+}},$$

which is translated into the ratio of branching fractions

$$\begin{aligned} R_{\psi(2S)/J/\psi} &\equiv \frac{\mathcal{B}(B_c^+ \rightarrow \psi(2S)\pi^+)}{\mathcal{B}(B_c^+ \rightarrow J/\psi\pi^+)} \\ &= F_{\psi(2S)/J/\psi} \cdot \frac{\mathcal{B}(J/\psi \rightarrow \mu^+ \mu^-)}{\mathcal{B}(\psi(2S) \rightarrow \mu^+ \mu^-)}. \end{aligned}$$

The branching fractions of the $J/\psi \rightarrow e^+ e^-$ and $\psi(2S) \rightarrow e^+ e^-$ decays are used in place of $\mathcal{B}(J/\psi \rightarrow \mu^+ \mu^-)$ and $\mathcal{B}(\psi(2S) \rightarrow \mu^+ \mu^-)$ because the branching fraction of electronic $\psi(2S)$ decays is more precisely measured than its muonic counterpart and the decay rates into $e^+ e^-$ and $\mu^+ \mu^-$ states are expected to be identical, up to negligible mass-dependent corrections, due to the universality of the electroweak couplings to charged leptons. The results are

$$\begin{aligned} F_{\psi(2S)/J/\psi} &= 0.0337 \pm 0.0024 (\text{stat}) \pm 0.0004 (\text{syst}), \\ R_{\psi(2S)/J/\psi} &= 0.254 \pm 0.018 (\text{stat}) \pm 0.003 (\text{syst}) \\ &\quad \pm 0.005 (\text{BF}), \end{aligned}$$

where for $R_{\psi(2S)/J/\psi}$ the third uncertainty is due to limited precision of the known branching fractions for J/ψ and $\psi(2S)$ leptonic decays [21]. The results are consistent with, but more precise than, those obtained in previous analyses [19,20]. As a cross check the values of $F_{\psi(2S)/J/\psi}$ and $R_{\psi(2S)/J/\psi}$ are determined at the $\pi^+ \mu^+ \mu^-$ WP, obtaining consistent results.

7 Summary

A search for nonresonant $B_c^+ \rightarrow \pi^+ \mu^+ \mu^-$ decays is performed together with an updated measurement of the ratio of the $B_c^+ \rightarrow \psi(2S)\pi^+$ and $B_c^+ \rightarrow J/\psi\pi^+$ branching fractions. The analysis uses proton–proton collision data collected with the LHCb detector between 2011 and 2018, corresponding to an integrated luminosity of 9 fb^{-1} . No evidence for an excess of signal events over background is observed for nonresonant $B_c^+ \rightarrow \pi^+ \mu^+ \mu^-$ decays and an upper limit is set on the branching fraction ratio

$$\frac{\mathcal{B}(B_c^+ \rightarrow \pi^+ \mu^+ \mu^-)}{\mathcal{B}(B_c^+ \rightarrow J/\psi\pi^+)} < 2.1 \times 10^{-4},$$

at 90% confidence level. This is the first limit on B_c^+ decays mediated only by annihilation diagrams into a semileptonic final state. For the resonant $B_c^+ \rightarrow \psi(2S)\pi^+$ mode, the branching fraction ratio is measured to be

$$\begin{aligned} \frac{\mathcal{B}(B_c^+ \rightarrow \psi(2S)\pi^+)}{\mathcal{B}(B_c^+ \rightarrow J/\psi\pi^+)} &= 0.254 \pm 0.018 (\text{stat}) \pm 0.003 (\text{syst}) \\ &\quad \pm 0.005 (\text{BF}), \end{aligned}$$

where the third uncertainty is due to limited precision of the known branching fractions for J/ψ and $\psi(2S)$ leptonic decays [21]. This measurement is consistent with, and surpasses, previous LHCb results on the same quantity [19,20] and is the most precise to date.

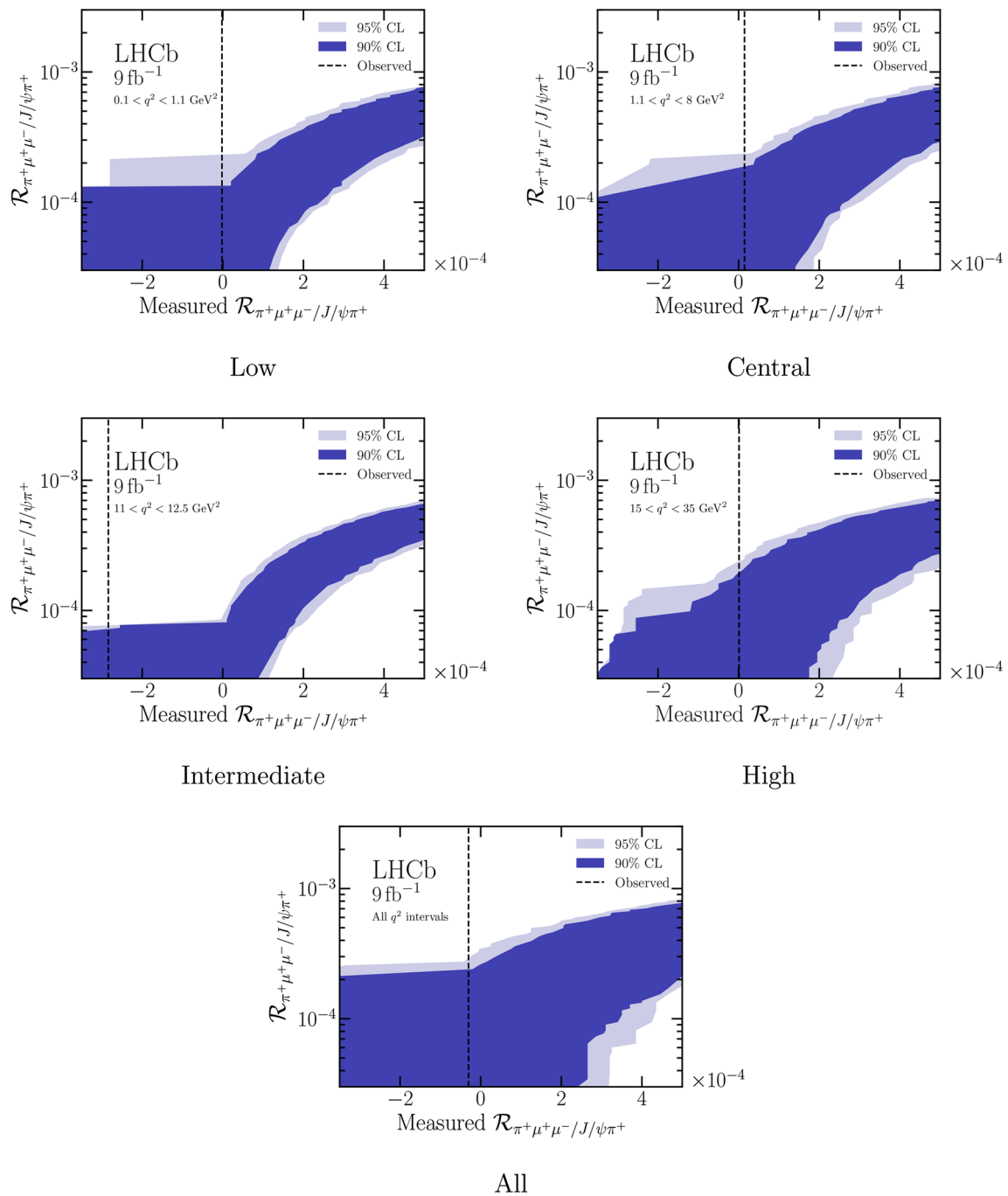
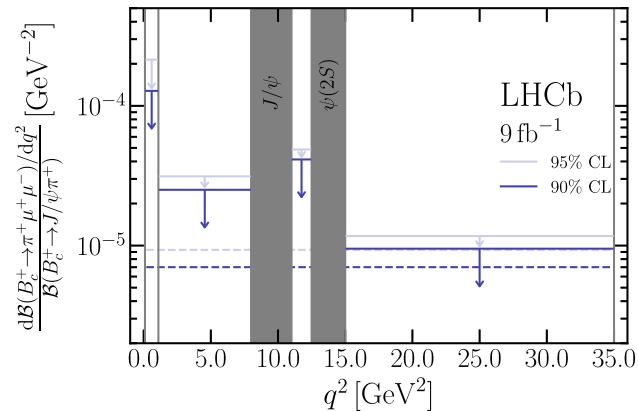


Fig. 5 Confidence belts generated using pseudoexperiments according to the Feldman–Cousins prescription [55] for each q^2 interval and for all intervals combined. The vertical dashed line shows the central value from the fit to data

Table 6 Results for $R_{\pi^+\mu^+\mu^-/J/\psi\pi^+}$, where the first uncertainties are statistical and the second are systematic, together with upper limits (ULs) at 90% and 95% CL

q^2 interval	$R_{\pi^+\mu^+\mu^-/J/\psi\pi^+}$	UL at 90% CL	UL at 95% CL
$0.1 < q^2 < 1.1 \text{ GeV}^2$	$(-0.2^{+4.8+0.8}_{-3.5-0.7}) \times 10^{-5}$	1.3×10^{-4}	2.1×10^{-4}
$1.1 < q^2 < 8.0 \text{ GeV}^2$	$(1.5^{+7.9+2.3}_{-6.4-1.4}) \times 10^{-5}$	1.7×10^{-4}	2.2×10^{-4}
$11.0 < q^2 < 12.5 \text{ GeV}^2$	$(-28.4^{+10.5+1.4}_{-16.1-1.7}) \times 10^{-5}$	0.6×10^{-4}	0.7×10^{-4}
$15.0 < q^2 < 35.0 \text{ GeV}^2$	$(0.2^{+11.5+3.4}_{-10.5-2.3}) \times 10^{-5}$	1.9×10^{-4}	2.3×10^{-4}
All	$(-3.0^{+15.0+2.4}_{-13.8-4.8}) \times 10^{-5}$	2.1×10^{-4}	2.7×10^{-4}

**Fig. 6** Upper limits on the normalised differential fraction for nonresonant $B_c^+ \rightarrow \pi^+\mu^+\mu^-$ decays as a function of q^2 . The solid lines show the results for each q^2 bin, while the dashed lines show the results for all bins combined

Acknowledgements We express our gratitude to our colleagues in the CERN accelerator departments for the excellent performance of the LHC. We thank the technical and administrative staff at the LHCb institutes. We acknowledge support from CERN and from the national agencies: CAPES, CNPq, FAPERJ and FINEP (Brazil); MOST and NSFC (China); CNRS/IN2P3 (France); BMBF, DFG and MPG (Germany); INFN (Italy); NWO (Netherlands); MNiSW and NCN (Poland); MCID/IFA (Romania); MICINN (Spain); SNSF and SER (Switzerland); NASU (Ukraine); STFC (United Kingdom); DOE NP and NSF (USA). We acknowledge the computing resources that are provided by CERN, IN2P3 (France), KIT and DESY (Germany), INFN (Italy), SURF (Netherlands), PIC (Spain), GridPP (United Kingdom), CSCS (Switzerland), IFIN-HH (Romania), CBPF (Brazil), and Polish WLCG (Poland). We are indebted to the communities behind the multiple open-source software packages on which we depend. Individual groups or members have received support from ARC and ARDC (Australia); Key Research Program of Frontier Sciences of CAS, CAS PIFI, CAS CCEPP, Fundamental Research Funds for the Central Universities, and Sci. & Tech. Program of Guangzhou (China); Minciencias (Colombia); EPLANET, Marie Skłodowska-Curie Actions, ERC and NextGenerationEU (European Union); A*MIDEX, ANR, IPhU and Labex P2IO, and Région Auvergne-Rhône-Alpes (France); AvH Foundation (Germany); ICSC (Italy); GVA, XuntaGal, GENCAT, Inditex, InTalent and Prog. Atracción Talento, CM (Spain); SRC (Sweden); the Leverhulme Trust, the Royal Society and UKRI (United Kingdom).

Data Availability Statement This manuscript has associated data in a data repository. [Author's comment: The LHCb experiment has agreed

to the CERN open data policy that is summarised in <https://opendata.cern.ch/docs/about>. In particular, Level 1 data associated with this publication are made available on the CERN document server at <http://cdsweb.cern.ch/record/2884481>. These data contain material related to the paper that allows a reinterpretation of the results in the context of new theoretical models. Level 3 data are also available from the CERN open data portal, but due to the large amount of data, only the Run 1 dataset has been made public up to now.]

Code Availability Statement Code/software cannot be made available for reasons disclosed in the code availability statement. [Author's comment: Software/Code that is associated with this publication and that is publicly available is referenced within the publication content. Specific analysis software/code used to produce the results shown in the publication is preserved within the LHCb collaboration internally and can be provided on reasonable request, provided it doesn't contain information that can be associated with unpublished results.]

Open Access This article is licensed under a Creative Commons Attribution 4.0 International License, which permits use, sharing, adaptation, distribution and reproduction in any medium or format, as long as you give appropriate credit to the original author(s) and the source, provide a link to the Creative Commons licence, and indicate if changes were made. The images or other third party material in this article are included in the article's Creative Commons licence, unless indicated otherwise in a credit line to the material. If material is not included in the article's Creative Commons licence and your intended use is not permitted by statutory regulation or exceeds the permitted use, you will need to obtain permission directly from the copyright holder. To view a copy of this licence, visit <http://creativecommons.org/licenses/by/4.0/>.
Funded by SCOAP³.

References

- LHCb collaboration, R. Aaij et al., Observation of the decay $B_c^+ \rightarrow B_s^0 \pi^+$. Phys. Rev. Lett. **111**, 181801 (2013). <https://doi.org/10.1103/PhysRevLett.111.181801>. arXiv:1308.4544
- LHCb collaboration, R. Aaij et al., Measurement of the ratio of branching fractions $B(B_c^+ \rightarrow B_s^0 \pi^+)/B(B_c^+ \rightarrow J/\psi \pi^+)$. JHEP **07**, 066 (2023). [https://doi.org/10.1007/JHEP07\(2023\)066](https://doi.org/10.1007/JHEP07(2023)066). arXiv:2210.12000
- A.G. Akeroyd, C.H. Chen, S. Recksiegel, Measuring $B^\pm \rightarrow \tau^\pm \nu$ and $B_c^\pm \rightarrow \tau^\pm \nu$ at the Z peak. Phys. Rev. D **77**, 115018 (2008). <https://doi.org/10.1103/PhysRevD.77.115018>. arXiv:0803.3517
- T. Zheng et al., Analysis of $B_c \rightarrow \tau \nu_\tau$ at CEPC. Chin. Phys. C **45**, 023001 (2021). <https://doi.org/10.1088/1674-1137/abc1f>. arXiv:2007.08234

5. Y. Amhis et al., Prospects for $B_c^+ \rightarrow \tau^+ \nu_\tau$ at FCC-ee. *JHEP* **12**, 133 (2021). [https://doi.org/10.1007/JHEP12\(2021\)133](https://doi.org/10.1007/JHEP12(2021)133). [arXiv:2105.13330](https://arxiv.org/abs/2105.13330)
6. M. Fedele et al., Prospects for B_c^+ and $B^+ \rightarrow \tau^+ \nu_\tau$ at FCC-ee. [arXiv:2305.02998](https://arxiv.org/abs/2305.02998)
7. LHCb collaboration, R. Aaij et al., Study of B_c^+ decays to the $K^+ K^- \pi^+$ final state and evidence for the decay $B_c^+ \rightarrow \chi_{c0} \pi^+$. *Phys. Rev. D* **94**, 091102(R) (2016). <https://doi.org/10.1103/PhysRevD.94.091102>. [arXiv:1607.06134](https://arxiv.org/abs/1607.06134)
8. LHCb collaboration, R. Aaij et al., Search for the suppressed decays $B^+ \rightarrow K^+ K^+ \pi^-$ and $B^+ \rightarrow \pi^+ \pi^+ K^-$. *Phys. Lett. B* **765**, 307 (2017). <https://doi.org/10.1016/j.physletb.2016.11.053>. [arXiv:1608.01478](https://arxiv.org/abs/1608.01478)
9. LHCb collaboration, R. Aaij et al., Observation of $B_c^+ \rightarrow D^0 K^+$ decays. *Phys. Rev. Lett.* **118**, 111803 (2017). <https://doi.org/10.1103/PhysRevLett.118.111803>. [arXiv:1701.01856](https://arxiv.org/abs/1701.01856)
10. LHCb collaboration, R. Aaij et al., A search for rare $B \rightarrow D \mu^+ \mu^-$ decays. *JHEP* **02**, 032 (2024). [https://doi.org/10.1007/JHEP02\(2024\)032](https://doi.org/10.1007/JHEP02(2024)032). [arXiv:2308.06162](https://arxiv.org/abs/2308.06162)
11. F. Abudinén, T. Blake, U. Egede, T. Gershon, Prospects for studies of $D^{*0} \rightarrow \mu^+ \mu^-$ and $B_{(s)}^{*0} \rightarrow \mu^+ \mu^-$ decays. *Eur. Phys. J. C* **82**, 459 (2022). <https://doi.org/10.1140/epjc/s10052-022-10369-y>. [arXiv:2202.03916](https://arxiv.org/abs/2202.03916)
12. A. Khodjamirian, T. Mannel, A.A. Petrov, Direct probes of flavor-changing neutral currents in $e^+ e^-$ -collisions. *JHEP* **11**, 142 (2015). [https://doi.org/10.1007/JHEP11\(2015\)142](https://doi.org/10.1007/JHEP11(2015)142). [arXiv:1509.07123](https://arxiv.org/abs/1509.07123)
13. B. Grinstein, J. Martin Camalich, Weak decays of excited B mesons. *Phys. Rev. Lett.* **116**, 141801 (2016). <https://doi.org/10.1103/PhysRevLett.116.141801>. [arXiv:1509.05049](https://arxiv.org/abs/1509.05049)
14. D.H. Evans, B. Grinstein, D.R. Nolte, Operator product expansion for exclusive decays: $B^+ \rightarrow D_s^+ e^+ e^-$ and $B^+ \rightarrow D_s^{*+} e^+ e^-$. *Phys. Rev. Lett.* **83**, 4947 (1999). <https://doi.org/10.1103/PhysRevLett.83.4947>. [arXiv:hep-ph/9904434](https://arxiv.org/abs/hep-ph/9904434)
15. M. Beneke, T. Feldmann, D. Seidel, Exclusive radiative and electroweak $b \rightarrow d$ and $b \rightarrow s$ penguin decays at NLO. *Eur. Phys. J. C* **41**, 173 (2005). <https://doi.org/10.1140/epjc/s2005-02181-5>. [arXiv:hep-ph/0412400](https://arxiv.org/abs/hep-ph/0412400)
16. W.-S. Hou, M. Kohda, F. Xu, Rates and asymmetries of $B \rightarrow \pi \ell^+ \ell^-$ decays. *Phys. Rev. D* **90**, 013002 (2014). <https://doi.org/10.1103/PhysRevD.90.013002>. [arXiv:1403.7410](https://arxiv.org/abs/1403.7410)
17. A. Ali, A. Parkhomenko, I. Parnova, Impact of weak annihilation contribution on rare semileptonic $B^+ \rightarrow \pi^+ \ell^+ \ell^-$ decay. *J. Phys. Conf. Ser.* **1690**, 012162 (2020). <https://doi.org/10.1088/1742-6596/1690/1/012162>
18. C.-D. Lü, Y.-L. Shen, C. Wang, Y.-M. Wang, Shedding new light on weak annihilation B-meson decays. *Nucl. Phys. B* **990**, 116175 (2023). <https://doi.org/10.1016/j.nuclphysb.2023.116175>. [arXiv:2202.08073](https://arxiv.org/abs/2202.08073)
19. LHCb collaboration, R. Aaij et al., Observation of the decay $B_c^+ \rightarrow \psi(2S) \pi^+$. *Phys. Rev. D* **87**, 071103(R) (2013). <https://doi.org/10.1103/PhysRevD.87.071103>. [arXiv:1303.1737](https://arxiv.org/abs/1303.1737)
20. LHCb collaboration, R. Aaij et al., Measurement of the branching fraction ratio $\mathcal{B}(B_c^+ \rightarrow \psi(2S) \pi^+) / \mathcal{B}(B_c^+ \rightarrow J/\psi \pi^+)$. *Phys. Rev. D* **92**, 057007 (2015). <https://doi.org/10.1103/PhysRevD.92.057007>. [arXiv:1507.03516](https://arxiv.org/abs/1507.03516)
21. Particle Data Group, R.L. Workman et al., Review of particle physics. *Prog. Theor. Exp. Phys.* **2022** 083C01 (2022). <https://doi.org/10.1093/ptep/ptac097>
22. LHCb collaboration, A.A. Alves Jr. et al., The LHCb detector at the LHC. *JINST* **3**, S08005 (2008). <https://doi.org/10.1088/1748-0221/3/08/S08005>
23. LHCb collaboration, R. Aaij et al., LHCb detector performance. *Int. J. Mod. Phys. A* **30**, 1530022 (2015). <https://doi.org/10.1142/S0217751X15300227>. [arXiv:1412.6352](https://arxiv.org/abs/1412.6352)
24. R. Aaij et al., Performance of the LHCb Vertex Locator. *JINST* **9**, P09007 (2014). <https://doi.org/10.1088/1748-0221/9/09/P09007>. [arXiv:1405.7808](https://arxiv.org/abs/1405.7808)
25. R. Arink et al., Performance of the LHCb Outer Tracker. *JINST* **9**, P01002 (2014). <https://doi.org/10.1088/1748-0221/9/01/P01002>. [arXiv:1311.3893](https://arxiv.org/abs/1311.3893)
26. P. d'Argent et al., Improved performance of the LHCb Outer Tracker in LHC Run 2. *JINST* **12**, P11016 (2017). <https://doi.org/10.1088/1748-0221/12/11/P11016>. [arXiv:1708.00819](https://arxiv.org/abs/1708.00819)
27. M. Adinolfi et al., Performance of the LHCb RICH detector at the LHC. *Eur. Phys. J. C* **73**, 2431 (2013). <https://doi.org/10.1140/epjc/s10052-013-2431-9>. [arXiv:1211.6759](https://arxiv.org/abs/1211.6759)
28. A.A. Alves Jr. et al., Performance of the LHCb muon system. *JINST* **8**, P02022 (2013). <https://doi.org/10.1088/1748-0221/8/02/P02022>. [arXiv:1211.1346](https://arxiv.org/abs/1211.1346)
29. R. Aaij et al., The LHCb trigger and its performance in 2011. *JINST* **8**, P04022 (2013). <https://doi.org/10.1088/1748-0221/8/04/P04022>. [arXiv:1211.3055](https://arxiv.org/abs/1211.3055)
30. R. Aaij et al., Performance of the LHCb trigger and full real-time reconstruction in Run 2 of the LHC. *JINST* **14**, P04013 (2019). <https://doi.org/10.1088/1748-0221/14/04/P04013>. [arXiv:1812.10790](https://arxiv.org/abs/1812.10790)
31. T. Sjöstrand, S. Mrenna, P. Skands, A brief introduction to PYTHIA 8.1. *Comput. Phys. Commun.* **178**, 852 (2008). <https://doi.org/10.1016/j.cpc.2008.01.036>. [arXiv:0710.3820](https://arxiv.org/abs/0710.3820)
32. I. Belyaev et al., Handling of the generation of primary events in Gauss, the LHCb simulation framework. *J. Phys. Conf. Ser.* **331**, 032047 (2011). <https://doi.org/10.1088/1742-6596/331/3/032047>
33. C.-H. Chang, J.-X. Wang, X.-G. Wu, BCVEGPy2.0: an upgraded version of the generator BCVEGPy with the addition of hadroproduction of the P-wave B_c^+ states. *Comput. Phys. Commun.* **174**, 241 (2006). <https://doi.org/10.1016/j.cpc.2005.09.008>. [arXiv:hep-ph/0504017](https://arxiv.org/abs/hep-ph/0504017)
34. D.J. Lange, The EvtGen particle decay simulation package. *Nucl. Instrum. Methods A* **462**, 152 (2001). [https://doi.org/10.1016/S0168-9002\(01\)00089-4](https://doi.org/10.1016/S0168-9002(01)00089-4)
35. N. Davidson, T. Przedzinski, Z. Was, PHOTOS interface in C++: technical and physics documentation. *Comput. Phys. Commun.* **199**, 86 (2016). <https://doi.org/10.1016/j.cpc.2015.09.013>. [arXiv:1011.0937](https://arxiv.org/abs/1011.0937)
36. Geant4 collaboration, J. Allison et al., Geant4 developments and applications. *IEEE Trans. Nucl. Sci.* **53**, 270 (2006). <https://doi.org/10.1109/TNS.2006.869826>
37. Geant4 collaboration, S. Agostinelli et al., Geant4: a simulation toolkit. *Nucl. Instrum. Methods A* **506**, 250 (2003). [https://doi.org/10.1016/S0168-9002\(03\)01368-8](https://doi.org/10.1016/S0168-9002(03)01368-8)
38. M. Clemencic et al., The LHCb simulation application, Gauss: design, evolution and experience. *J. Phys. Conf. Ser.* **331**, 032023 (2011). <https://doi.org/10.1088/1742-6596/331/3/032023>
39. D. Müller, M. Clemencic, G. Corti, M. Gersabeck, ReDecay: a novel approach to speed up the simulation at LHCb. *Eur. Phys. J. C* **78**, 1009 (2018). <https://doi.org/10.1140/epjc/s10052-018-6469-6>. [arXiv:1810.10362](https://arxiv.org/abs/1810.10362)
40. R. Aaij et al., Selection and processing of calibration samples to measure the particle identification performance of the LHCb experiment in Run 2. *Eur. Phys. J. Tech. Instr.* **6**, 1 (2019). <https://doi.org/10.1140/epjti/s40485-019-0050-z>. [arXiv:1803.00824](https://arxiv.org/abs/1803.00824)
41. LHCb collaboration, R. Aaij et al., Measurement of the track reconstruction efficiency at LHCb. *JINST* **10**, P02007 (2015). <https://doi.org/10.1088/1748-0221/10/02/P02007>. [arXiv:1408.1251](https://arxiv.org/abs/1408.1251)
42. S. Tolk, J. Albrecht, F. Dettori, A. Pellegrino, Data driven trigger efficiency determination at LHCb. LHCb-PUB-2014-039 (2014)
43. LHCb collaboration, R. Aaij et al., Measurement of the B_c^+ meson lifetime using $B_c^+ \rightarrow J/\psi \mu^+ \nu_\mu X$ decays. *Eur. Phys. J. C* **74**, 2839 (2014). <https://doi.org/10.1140/epjc/s10052-014-2839-x>. [arXiv:1401.6932](https://arxiv.org/abs/1401.6932)

44. LHCb collaboration, R. Aaij et al., Measurement of the lifetime of the B_c^+ meson using the $B_c^+ \rightarrow J/\psi\pi^+$ decay mode. *Phys. Lett. B* **742**, 29 (2015). <https://doi.org/10.1016/j.physletb.2015.01.010>. arXiv:1411.6899
45. A. Rogozhnikov, Reweighting with boosted decision trees. *J. Phys. Conf. Ser.* **762**, 012036 (2016). <https://doi.org/10.1088/1742-6596/762/1/012036>. arXiv:1608.05806
46. LHCb collaboration, R. Aaij et al., Search for $D^{*0} \rightarrow \mu^+\mu^-$ in $B^- \rightarrow \pi^-\mu^+\mu^-$ decays. *Eur. Phys. J. C* **83**, 666 (2023). <https://doi.org/10.1140/epjc/s10052-023-11759-6>. arXiv:2304.01981
47. V.V. Gligorov, M. Williams, Efficient, reliable and fast high-level triggering using a bonsai boosted decision tree. *JINST* **8**, P02013 (2013). <https://doi.org/10.1088/1748-0221/8/02/P02013>. arXiv:1210.6861
48. T. Likhomanenko et al., LHCb topological trigger reoptimization. *J. Phys. Conf. Ser.* **664**, 082025 (2015). <https://doi.org/10.1088/1742-6596/664/8/082025>
49. L. Breiman, J.H. Friedman, R.A. Olshen, C.J. Stone, *Classification and Regression Trees* (Wadsworth International Group, Belmont, 1984)
50. T. Chen, C. Guestrin, XGBoost: a scalable tree boosting system, in *Proceedings of the 22nd ACM SIGKDD International Conference on Knowledge Discovery and Data Mining*, KDD '16, (New York) (ACM, 2016), p. 785–794. <https://doi.org/10.1145/2939672.2939785>
51. G. Punzi, Sensitivity of searches for new signals and its optimization. eConf **C030908** (2003) MODT002, arXiv:physics/0308063
52. LHCb collaboration, R. Aaij et al., Measurement of the ratio of branching fractions $B(B_c^+ \rightarrow J/\psi K^+)/B(B_c^+ \rightarrow J/\psi\pi^+)$. *JHEP* **09**, 153 (2016). [https://doi.org/10.1007/JHEP09\(2016\)153](https://doi.org/10.1007/JHEP09(2016)153). arXiv:1607.06823
53. T. Skwarnicki, A study of the radiative cascade transitions between the Upsilon-prime and Upsilon resonances, Ph.D. thesis, Institute of Nuclear Physics, Krakow, DESY-F31-86-02 (1986)
54. I. Narsky, F. Porter, *Statistical Analysis Techniques in Particle Physics: Fits, Density Estimation and Supervised Learning* (Wiley, 2013). Likelihood fits with low statistics are discussed in Sec. 2.3.2. <https://doi.org/10.1002/9783527677320>
55. G.J. Feldman, R.D. Cousins, A unified approach to the classical statistical analysis of small signals. *Phys. Rev. D* **57**, 3873 (1998). <https://doi.org/10.1103/PhysRevD.57.3873>. arXiv:physics/9711021

LHCb Collaboration

R. Aaij³⁵, A.S.W. Abdelmotteleb⁵⁴, C. Abellan Beteta⁴⁸, F. Abudinén^{54,*}, T. Ackernley⁵⁸, B. Adeva⁴⁴, M. Adinolfi⁵², P. Adlarson⁷⁸, C. Agapopoulou⁴⁶, C. A. Aidala⁷⁹, Z. Ajaltouni¹¹, S. Akar⁶³, K. Akiba³⁵, P. Albicocco²⁵, J. Albrecht¹⁷, F. Alessio⁴⁶, M. Alexander⁵⁷, A. Alfonso Albero⁴³, Z. Aliouche⁶⁰, P. Alvarez Cartelle⁵³, R. Amalric¹⁵, S. Amato³, J. L. Amey⁵², Y. Amhis^{13,46}, L. An⁶, L. Anderlini²⁴, M. Andersson⁴⁸, A. Andreianov⁴¹, P. Andreola⁴⁸, M. Andreotti²³, D. Andreou⁶⁶, A. Anelli^{28,o}, D. Ao⁷, F. Archilli^{34,u}, M. Argenton²³, S. Arguedas Cuendis⁹, A. Artamonov⁴¹, M. Artuso⁶⁶, E. Aslanides¹², M. Atzeni⁶², B. Audurier¹⁴, D. Bacher⁶¹, I. Bachiller Perea¹⁰, S. Bachmann¹⁹, M. Bachmayer⁴⁷, J. J. Back⁵⁴, P. Baladron Rodriguez⁴⁴, V. Balagura¹⁴, W. Baldini²³, J. Baptista de Souza Leite², M. Barbetti^{24,l}, I. R. Barbosa⁶⁷, R.J. Barlow⁶⁰, S. Barsuk¹³, W. Barter⁵⁶, M. Bartolini⁵³, J. Bartz⁶⁶, F. Baryshnikov⁴¹, J. M. Basels¹⁶, G. Bassi^{32,r}, B. Batsukh⁵, A. Battig¹⁷, A. Bay⁴⁷, A. Beck⁵⁴, M. Becker¹⁷, F. Bedeschi³², I. B. Bediaga², A. Beiter⁶⁶, S. Belin⁴⁴, V. Bellec⁴⁸, K. Belous⁴¹, I. Belov²⁶, I. Belyaev⁴¹, G. Benane¹², G. Bencivenni²⁵, E. Ben-Haim¹⁵, A. Berezhnoy⁴¹, R. Bernet⁴⁸, S. Bernet Andres⁴², C. Bertella⁶⁰, A. Bertolin³⁰, C. Betancourt⁴⁸, F. Betti⁵⁶, J. Bex⁵³, Ia. Bezshyiko⁴⁸, J. Bhom³⁸, M. S. Bieker¹⁷, N. V. Biesuz²³, P. Billoir¹⁵, A. Biolchini³⁵, M. Birch⁵⁹, F. C. R. Bishop¹⁰, A. Bitadze⁶⁰, A. Bizzeti, M. P. Blago⁵³, T. Blake⁵⁴, F. Blanc⁴⁷, J. E. Blank¹⁷, S. Blusk⁶⁶, D. Bobulska⁵⁷, V. Bocharnikov⁴¹, J. A. Boelhaue¹⁷, O. Boente Garcia¹⁴, T. Boettcher⁶³, A. Bohare⁵⁶, A. Boldyrev⁴¹, C. S. Bolognani⁷⁶, R. Bolzonella^{23,k}, N. Bondar⁴¹, F. Borgato^{30,46}, S. Borghi⁶⁰, M. Borsato^{28,o}, J. T. Borsuk³⁸, S. A. Bouchiba⁴⁷, T. J. V. Bowcock⁵⁸, A. Boyer⁴⁶, C. Bozzi²³, M. J. Bradley⁵⁹, A. Brea Rodriguez⁴⁴, N. Breer¹⁷, J. Brodzicka³⁸, A. Brossa Gonzalo⁴⁴, J. Brown⁵⁸, D. Brundu²⁹, A. Buonauro⁴⁸, L. Buonincontri³⁰, A. T. Burke⁶⁰, C. Burr⁴⁶, A. Bursche⁶⁹, A. Butkevich⁴¹, J. S. Butter⁵³, J. Buytaert⁴⁶, W. Byczynski⁴⁶, S. Cadeddu²⁹, H. Cai⁷¹, R. Calabrese^{23,k}, L. Caffice¹⁷, S. Cali²⁵, M. Calvi^{28,o}, M. Calvo Gomez⁴², J. Cambon Bouzas⁴⁴, P. Campana²⁵, D. H. Campora Perez⁷⁶, A.F. Campoverde Quezada⁷, S. Capelli^{28,o}, L. Capriotti²³, R. Caravaca-Mora⁹, A. Carbone^{22,i}, L. Carcedo Salgado⁴⁴, R. Cardinale^{26,m}, A. Cardini²⁹, P. Carniti^{28,o}, L. Carus¹⁹, A. Casais Vidal⁶², R. Caspary¹⁹, G. Casse⁵⁸, J. Castro Godinez⁹, M. Cattaneo⁴⁶, G. Cavallero²³, V. Cavallini^{23,k}, S. Celani¹⁹, J. Cerasoli¹², D. Cervenkov⁶¹, S. Cesare^{27,n}, A. J. Chadwick⁵⁸, I. Chahrouh⁷⁹, M. Charles¹⁵, Ph. Charpentier⁴⁶, C. A. Chavez Barajas⁵⁸, M. Chefdeville¹⁰, C. Chen¹², S. Chen⁵, Z. Chen⁷, A. Chernov³⁸, S. Chernyshenko⁵⁰, V. Chobanova^{44,y}, S. Cholak⁴⁷, M. Chrzaszcz³⁸, A. Chubykin⁴¹, V. Chulikov⁴¹, P. Ciambone²⁵, M. F. Cicala⁵⁴, X. Cid Vidal⁴⁴,

G. Ciezarek⁴⁶, P. Cifra⁴⁶, P. E. L. Clarke⁵⁶, M. Clemencic⁴⁶, H. V. Cliff⁵³, J. Closier⁴⁶, J. L. Cobbley⁶⁰, C. Cocha Toapaxi¹⁹, V. Coco⁴⁶, J. Cogan¹², E. Cogneras¹¹, L. Cojocariu⁴⁰, P. Collins⁴⁶, T. Colombo⁴⁶, A. Comerma-Montells⁴³, L. Congedo²¹, A. Contu²⁹, N. Cooke⁵⁷, I. Corredoira⁴⁴, A. Correia¹⁵, G. Corti⁴⁶, J. J. Cottee Meldrum⁵², B. Couturier⁴⁶, D. C. Craik⁴⁸, M. Cruz Torres^{2.g}, E. Curras Rivera⁴⁷, R. Currie⁵⁶, C. L. Da Silva⁶⁵, S. Dadabaev⁴¹, L. Dai⁶⁸, X. Dai⁶, E. Dall'Occo¹⁷, J. Dalseno⁴⁴, C. D'Ambrosio⁴⁶, J. Daniel¹¹, A. Danilina⁴¹, P. d'Argent²¹, A. Davidson⁵⁴, J. E. Davies⁶⁰, A. Davis⁶⁰, O. De Aguiar Francisco⁶⁰, C. De Angelis^{29.j}, J. de Boer³⁵, K. De Bruyn⁷⁵, S. De Capua⁶⁰, M. De Cian^{19.46}, U. De Freitas Carneiro Da Graca^{2.b}, E. De Lucia²⁵, J. M. De Miranda², L. De Paula³, M. De Serio^{21.h}, D. De Simone⁴⁸, P. De Simone²⁵, F. De Vellis¹⁷, J. A. de Vries⁷⁶, F. Debernardis^{21.h}, D. Decamp¹⁰, V. Dedu¹², L. Del Buono¹⁵, B. Delaney⁶², H.-P. Dembinski¹⁷, J. Deng⁸, V. Denysenko⁴⁸, O. Deschamps¹¹, F. Dettori^{29.j}, B. Dey⁷⁴, P. Di Nezza²⁵, I. Diachkov⁴¹, S. Didenko⁴¹, S. Ding⁶⁶, V. Dobishuk⁵⁰, A. D. Docheva⁵⁷, A. Dolmatov⁴¹, C. Dong⁴, A. M. Donohoe²⁰, F. Dordei²⁹, A. C. dos Reis², L. Douglas⁵⁷, A. G. Downes¹⁰, W. Duan⁶⁹, P. Duda⁷⁷, M. W. Dudek³⁸, L. Dufour⁴⁶, V. Duk³¹, P. Durante⁴⁶, M. M. Duras⁷⁷, J. M. Durham⁶⁵, A. Dziurda³⁸, A. Dzyuba⁴¹, S. Easo^{55.46}, E. Eckstein⁷³, U. Egede¹, A. Egorychev⁴¹, V. Egorychev⁴¹, C. Eirea Orro⁴⁴, S. Eisenhardt⁵⁶, E. Ejopu⁶⁰, S. Ek-In⁴⁷, L. Eklund⁷⁸, M. Elashri⁶³, J. Ellbracht¹⁷, S. Ely⁵⁹, A. Ene⁴⁰, E. Eppe⁶³, S. Escher¹⁶, J. Eschle⁴⁸, S. Esen¹⁹, T. Evans⁶⁰, F. Fabiano^{29.j.46}, L. N. Falcao², Y. Fan⁷, B. Fang^{71.13}, L. Fantini^{31.q}, M. Faria⁴⁷, K. Farmer⁵⁶, D. Fazzini^{28.o}, L. Felkowski⁷⁷, M. Feng^{5.7}, M. Feo⁴⁶, M. Fernandez Gomez⁴⁴, A. D. Fernez⁶⁴, F. Ferrari²², F. Ferreira Rodrigues³, S. Ferreres Sole³⁵, M. Ferrillo⁴⁸, M. Ferro-Luzzi⁴⁶, S. Filippov⁴¹, R. A. Fini²¹, M. Fiorini^{23.k}, K. M. Fischer⁶¹, D. S. Fitzgerald⁷⁹, C. Fitzpatrick⁶⁰, F. Fleuret¹⁴, M. Fontana²², L. F. Foreman⁶⁰, R. Forty⁴⁶, D. Foulds-Holt⁵³, M. Franco Sevilla⁶⁴, M. Frank⁴⁶, E. Franzoso^{23.k}, G. Frau¹⁹, C. Frei⁴⁶, D. A. Friday⁶⁰, L. Frontini²⁷, J. Fu⁷, Q. Fuehring¹⁷, Y. Fujii¹, T. Fulghesu¹⁵, E. Gabriel³⁵, G. Galati^{21.h}, M. D. Galati³⁵, A. Gallas Torreira⁴⁴, D. Galli^{22.i}, S. Gambetta⁵⁶, M. Gandelman³, P. Gandini²⁷, H. Gao⁷, R. Gao⁶¹, Y. Gao⁸, Y. Gao⁶, Y. Gao⁸, M. Garau^{29.j}, L. M. Garcia Martin⁴⁷, P. Garcia Moreno⁴³, J. García Pardiñas⁴⁶, B. Garcia Plana⁴⁴, K. G. Garg⁸, L. Garrido⁴³, C. Gaspar⁴⁶, R. E. Geertsema³⁵, L. L. Gerken¹⁷, E. Gersabeck⁶⁰, M. Gersabeck⁶⁰, T. Gershon⁵⁴, Z. Ghorbanimoghaddam⁵², L. Giambastiani³⁰, F. I. Giasemis^{15.e}, V. Gibson⁵³, H. K. Gienza³⁹, A. L. Gilman⁶¹, M. Giovannetti²⁵, A. Gioventù⁴³, P. Gironella Gironell⁴³, C. Giugliano^{23.k}, M. A. Giza³⁸, E. L. Gkougkousis⁵⁹, F. C. Glaser^{13.19}, V. V. Gligorov¹⁵, C. Göbel⁶⁷, E. Golobardes⁴², D. Golubkov⁴¹, A. Golutvin^{59.41.46}, A. Gomes^{2.a,*}, S. Gomez Fernandez⁴³, F. Goncalves Abrantes⁶¹, M. Goncerz³⁸, G. Gong⁴, J. A. Gooding¹⁷, I. V. Gorelov⁴¹, C. Gotti²⁸, J. P. Grabowski⁷³, L. A. Granado Cardoso⁴⁶, E. Graugés⁴³, E. Graverini^{47.s}, L. Grazette⁵⁴, G. Graziani, A. T. Grecu⁴⁰, L. M. Greeven³⁵, N. A. Grieser⁶³, L. Grillo⁵⁷, S. Gromov⁴¹, C. Gu¹⁴, M. Guarise²³, M. Guittiere¹³, V. Guliaeva⁴¹, P. A. Günther¹⁹, A.-K. Guseinov⁴¹, E. Gushchin⁴¹, Y. Guz^{6.41.46}, T. Gys⁴⁶, K. Habermann⁷³, T. Hadavizadeh¹, C. Hadjivasiliou⁶⁴, G. Haefeli⁴⁷, C. Haen⁴⁶, J. Haimberger⁴⁶, M. Hajheidari⁴⁶, M. M. Halvorsen⁴⁶, P. M. Hamilton⁶⁴, J. Hammerich⁵⁸, Q. Han⁸, X. Han¹⁹, S. Hansmann-Menzemer¹⁹, L. Hao⁷, N. Harnew⁶¹, T. Harrison⁵⁸, M. Hartmann¹³, J. He^{7.c}, K. Heijhoff³⁵, F. Hemmer⁴⁶, C. Henderson⁶³, R. D. L. Henderson^{1.54}, A. M. Hennequin⁴⁶, K. Hennessy⁵⁸, L. Henry⁴⁷, J. Herd⁵⁹, P. Herrero Gascon¹⁹, J. Heuel¹⁶, A. Hicheur³, G. Hijano Mendizabal⁴⁸, D. Hill⁴⁷, S. E. Hollitt¹⁷, J. Horswill⁶⁰, R. Hou⁸, Y. Hou¹⁰, N. Howarth⁵⁸, J. Hu¹⁹, J. Hu⁶⁹, W. Hu⁶, X. Hu⁴, W. Huang⁷, W. Hulsbergen³⁵, R. J. Hunter⁵⁴, M. Hushchyn⁴¹, D. Hutchcroft⁵⁸, D. Ilin⁴¹, P. Ilten⁶³, A. Inglessi⁴¹, A. Iniukhin⁴¹, A. Ishteev⁴¹, K. Ivshin⁴¹, R. Jacobsson⁴⁶, H. Jage¹⁶, S. J. Jaimes Elles^{45.72}, S. Jakobsen⁴⁶, E. Jans³⁵, B. K. Jashal⁴⁵, A. Jawahery^{64.46}, V. Jevtic¹⁷, E. Jiang⁶⁴, X. Jiang^{5.7}, Y. Jiang⁷, Y. J. Jiang⁶, M. John⁶¹, D. Johnson⁵¹, C. R. Jones⁵³, T. P. Jones⁵⁴, S. Joshi³⁹, B. Jost⁴⁶, N. Jurik⁴⁶, I. Juszczak³⁸, D. Kaminaris⁴⁷, S. Kandybei⁴⁹, Y. Kang⁴, M. Karacson⁴⁶, D. Karpenkov⁴¹, M. Karpov⁴¹, A. M. Kauniskangas⁴⁷, J. W. Kautz⁶³, F. Keizer⁴⁶, D. M. Keller⁶⁶, M. Kenzie⁵³, T. Ketel³⁵, B. Khanji⁶⁶, A. Kharisova⁴¹, S. Kholodenko³², G. Khreich¹³, T. Kirn¹⁶, V. S. Kirsebom⁴⁷, O. Kitouni⁶², S. Klaver³⁶, N. Klejne^{32.r}, K. Klimaszewski³⁹, M. R. Kmiec³⁹, S. Koliiev⁵⁰, L. Kolk¹⁷, A. Konoplyannikov⁴¹, P. Kopciwicz^{37.46}, P. Koppenburg³⁵, M. Korolev⁴¹, I. Kostiuik³⁵, O. Kot⁵⁰, S. Kotriakhova, A. Kozachuk⁴¹, P. Kravchenko⁴¹, L. Kravchuk⁴¹, M. Kreps⁵⁴, S. Kretzschmar¹⁶, P. Krokovny⁴¹, W. Krupa⁶⁶, W. Krzemien³⁹, J. Kubat¹⁹, S. Kubis⁷⁷, W. Kucewicz³⁸, M. Kucharczyk³⁸, V. Kudryavtsev⁴¹, E. Kulikova⁴¹, A. Kupsc⁷⁸, B. K. Kutsenko¹², D. Lacarrere⁴⁶, A. Lai²⁹, A. Lampis²⁹, D. Lancierini⁴⁸, C. Landesa Gomez⁴⁴, J. J. Lane¹, R. Lane⁵², C. Langenbruch¹⁹, J. Langer¹⁷, O. Lantwin⁴¹, T. Latham⁵⁴, F. Lazzari^{32.s}, C. Lazzeroni⁵¹, R. Le Gac¹², S. H. Lee⁷⁹,

R. Lefèvre¹¹, A. Leflat⁴¹, S. Legotin⁴¹, M. Lehuraux⁵⁴, O. Leroy¹², T. Lesiak³⁸, B. Leverington¹⁹, A. Li⁴, H. Li⁶⁹, K. Li⁸, L. Li⁶⁰, P. Li⁴⁶, P.-R. Li⁷⁰, S. Li⁸, T. Li^{5,d}, T. Li⁶⁹, Y. Li⁸, Y. Li⁵, Z. Li⁶⁶, Z. Lian⁴, X. Liang⁶⁶, C. Lin⁷, T. Lin⁵⁵, R. Lindner⁴⁶, V. Lisovskyi⁴⁷, R. Litvinov^{29,j}, F. L. Liu¹, G. Liu⁶⁹, K. Liu⁷⁰, Q. Liu⁷, S. Liu^{5,7}, Y. Liu⁵⁶, Y. Liu⁷⁰, Y. L. Liu⁵⁹, A. Lobo Salvia⁴³, A. Loi²⁹, J. Lomba Castro⁴⁴, T. Long⁵³, J. H. Lopes³, A. Lopez Huertas⁴³, S. L.ópez Soliño⁴⁴, G. H. Lovell⁵³, C. Lucarelli^{24,1}, D. Lucchesi^{30,p}, S. Luchuk⁴¹, M. Lucio Martinez⁷⁶, V. Lukashenko^{35,50}, Y. Luo⁶, A. Lupato³⁰, E. Luppi^{23,k}, K. Lynch²⁰, X.-R. Lyu⁷, G. M. Ma⁴, R. Ma⁷, S. Maccolini¹⁷, F. Machefert¹³, F. Maciuc⁴⁰, B. M. Mack⁶⁶, I. Mackay⁶¹, L. M. Mackey⁶⁶, L. R. Madhan Mohan⁵³, M. M. Madurai⁵¹, A. Maevskiy⁴¹, D. Magdalinski³⁵, V. Mahajan⁵⁴, D. Maisuzenko⁴¹, M. W. Majewski³⁷, J. J. Malczewski³⁸, S. Malde⁶¹, B. Malecki^{38,46}, L. Malentacca⁴⁶, A. Malinin⁴¹, T. Maltsev⁴¹, G. Manca^{29,j}, G. Mancinelli¹², C. Mancuso^{13,27,n}, R. Manera Escalero⁴³, D. Manuzzi²², D. Marangotto^{27,n}, J. F. Marchand¹⁰, R. Marchevski⁴⁷, U. Marconi²², S. Mariani⁴⁶, C. Marin Benito⁴³, J. Marks¹⁹, A. M. Marshall⁵², P. J. Marshall⁵⁸, G. Martelli^{31,q}, G. Martellotti³³, L. Martinazzoli⁴⁶, M. Martinelli^{28,o}, D. Martinez Santos⁴⁴, F. Martinez Vidal⁴⁵, A. Massafferri², M. Materok¹⁶, R. Matev⁴⁶, A. Mathad⁴⁸, V. Matiunin⁴¹, C. Matteuzzi⁶⁶, K. R. Mattioli¹⁴, A. Mauri⁵⁹, E. Maurice¹⁴, J. Mauricio⁴³, P. Mayencourt⁴⁷, M. Mazurek⁴⁶, M. McCann⁵⁹, L. McConnell²⁰, T. H. McGrath⁶⁰, N. T. McHugh⁵⁷, A. McNab⁶⁰, R. McNulty²⁰, B. Meadows⁶³, G. Meier¹⁷, D. Melnychuk³⁹, M. Merk^{35,76}, A. Merli^{27,n}, L. Meyer Garcia³, D. Miao^{5,7}, H. Miao⁷, M. Mikhasenko^{73,f}, D. A. Milanes⁷², A. Minotti^{28,o}, E. Minucci⁶⁶, T. Miralles¹¹, S. E. Mitchell⁵⁶, B. Mitreska¹⁷, D. S. Mitzel¹⁷, A. Modak⁵⁵, A. Mödden¹⁷, R. A. Mohammed⁶¹, R. D. Moise¹⁶, S. Mikhnenko⁴¹, T. Mombächer⁴⁶, M. Monk^{54,1}, I. A. Monroy⁷², S. Monteil¹¹, A. Morcillo Gomez⁴⁴, G. Morello²⁵, M. J. Morello^{32,r}, M. P. Morgenthaler¹⁹, A. B. Morris⁴⁶, A. G. Morris¹², R. Mountain⁶⁶, H. Mu⁴, Z. M. Mu⁶, E. Muhammad⁵⁴, F. Muheim⁵⁶, M. Mulder⁷⁵, K. Müller⁴⁸, F. Muñoz-Rojas⁹, R. Murta⁵⁹, P. Naik⁵⁸, T. Nakada⁴⁷, R. Nandakumar⁵⁵, T. Nanut⁴⁶, I. Nasteva³, M. Needham⁵⁶, N. Neri^{27,n}, S. Neubert⁷³, N. Neufeld⁴⁶, P. Neustroev⁴¹, R. Newcombe⁵⁹, J. Nicolini^{13,17}, D. Nicotra⁷⁶, E. M. Niel⁴⁷, N. Nikitin⁴¹, P. Nogga⁷³, N. S. Nolte⁶², C. Normand^{10,29}, J. Novoa Fernandez⁴⁴, G. Nowak⁶³, C. Nunez⁷⁹, H. N. Nur⁵⁷, A. Oblakowska-Mucha³⁷, V. Obraztsov⁴¹, T. Oeser¹⁶, S. Okamura^{23,k,46}, R. Oldeman^{29,j}, F. Oliva⁵⁶, M. Olocco¹⁷, C. J. G. Onderwater⁷⁶, R. H. O'Neil⁵⁶, J. M. Otorola Goicochea³, T. Ovsianikova⁴¹, P. Owen⁴⁸, A. Oyanguren⁴⁵, O. Ozcelik⁵⁶, K. O. Padeken⁷³, B. Pagare⁵⁴, P. R. Pais¹⁹, T. Pajero⁶¹, A. Palano²¹, M. Palutan²⁵, G. Panshin⁴¹, L. Paolucci⁵⁴, A. Papanestis⁵⁵, M. Pappagallo^{21,h}, L. L. Pappalardo^{23,k}, C. Pappenheimer⁶³, C. Parkes⁶⁰, B. Passalacqua^{23,k}, G. Passaleva²⁴, D. Passaro^{32,r}, A. Pastore²¹, M. Patel⁵⁹, J. Patoc⁶¹, C. Patrignani^{22,i}, C. J. Pawley⁷⁶, A. Pellegrino³⁵, M. Pepe Altarelli²⁵, S. Perazzini²², D. Pereima⁴¹, A. Pereiro Castro⁴⁴, P. Perret¹¹, A. Perro⁴⁶, K. Petridis⁵², A. Petrolini^{26,m}, S. Petrucci⁵⁶, J. P. Pfaller⁶³, H. Pham⁶⁶, L. Pica^{32,r}, M. Piccini³¹, B. Pietrzyk¹⁰, G. Pietrzyk¹³, D. Pinci³³, F. Pisani⁴⁶, M. Pizzichemi^{28,o}, V. Placinta⁴⁰, M. Plo Casasus⁴⁴, F. Polci^{15,46}, M. Poli Lener²⁵, A. Poluektov¹², N. Polukhina⁴¹, I. Polyakov⁴⁶, E. Polycarpo³, S. Ponce⁴⁶, D. Popov⁷, S. Poslavskii⁴¹, K. Prasanth³⁸, C. Prouve⁴⁴, V. Pugatch⁵⁰, G. Punzi^{32,s}, W. Qian⁷, N. Qin⁴, S. Qu⁴, R. Quagliani⁴⁷, R. I. Rabadan Trejo⁵⁴, J. H. Rademacker⁵², M. Rama³², M. Ramírez García⁷⁹, M. Ramos Pernas⁵⁴, M. S. Rangel³, F. Ratnikov⁴¹, G. Raven³⁶, M. Rebollo De Miguel⁴⁵, F. Redi⁴⁶, J. Reich⁵², F. Reiss⁶⁰, Z. Ren⁷, P. K. Resmi⁶¹, R. Ribatti^{32,r}, G. R. Ricart^{14,80}, D. Ricciardi^{32,r}, S. Ricciardi⁵⁵, K. Richardson⁶², M. Richardson-Slipper⁵⁶, K. Rinnert⁵⁸, P. Robbe¹³, G. Robertson⁵⁷, E. Rodrigues^{58,46}, E. Rodriguez Fernandez⁴⁴, J. A. Rodriguez Lopez⁷², E. Rodriguez Rodriguez⁴⁴, A. Rogovskiy⁵⁵, D. L. Rolf⁴⁶, A. Rollings⁶¹, P. Roloff⁴⁶, V. Romanovskiy⁴¹, M. Romero Lamas⁴⁴, A. Romero Vidal⁴⁴, G. Romolini²³, F. Ronchetti⁴⁷, M. Rotondo²⁵, S. R. Roy¹⁹, M. S. Rudolph⁶⁶, T. Ruf⁴⁶, M. Ruiz Diaz¹⁹, R. A. Ruiz Fernandez⁴⁴, J. Ruiz Vidal^{78,z}, A. Ryzhikov⁴¹, J. Ryzka³⁷, J. J. Saborido Silva⁴⁴, R. Sadek¹⁴, N. Sagidova⁴¹, N. Sahoo⁵¹, B. Saitta^{29,j}, M. Salomoni^{28,o}, C. Sanchez Gras³⁵, I. Sanderswood⁴⁵, R. Santacesaria³³, C. Santamarina Rios⁴⁴, M. Santimaria²⁵, L. Santoro², E. Santovetti³⁴, A. Saputi^{23,46}, D. Saranin⁴¹, G. Sarpis⁵⁶, M. Sarpis⁷³, A. Sarti³³, C. Satriano^{33,t}, A. Satta³⁴, M. Saur⁶, D. Savrina⁴¹, H. Sazak¹¹, L. G. Scantlebury Smead⁶¹, A. Scarabotto¹⁵, S. Schael¹⁶, S. Scherl⁵⁸, A. M. Schertz⁷⁴, M. Schiller⁵⁷, H. Schindler⁴⁶, M. Schmelling¹⁸, B. Schmidt⁴⁶, S. Schmitt¹⁶, H. Schmitz⁷³, O. Schneider⁴⁷, A. Schopper⁴⁶, N. Schulte¹⁷, S. Schulte⁴⁷, M. H. Schune¹³, R. Schwemmer⁴⁶, G. Schwering¹⁶, B. Sciascia²⁵, A. Sciucchi⁴⁶, S. Sellam⁴⁴, A. Semennikov⁴¹, M. Senghi Soares³⁶, A. Sergi^{26,m}, N. Serra^{48,46}, L. Sestini³⁰, A. Seuthe¹⁷, Y. Shang⁶, D. M. Shangase⁷⁹, M. Shapkin⁴¹, R. S. Sharma⁶⁶, I. Shchemerov⁴¹, L. Shchutska⁴⁷, T. Shears⁵⁸, L. Shekhtman⁴¹

Z. Shen⁶, S. Sheng^{5,7}, V. Shevchenko⁴¹, B. Shi⁷, E. B. Shields^{28,o}, Y. Shimizu¹³, E. Shmanin⁴¹, R. Shorkin⁴¹, J. D. Shupperd⁶⁶, R. Silva Coutinho⁶⁶, G. Simi³⁰, S. Simone^{21,h}, N. Skidmore⁵⁴, R. Skuza¹⁹, T. Skwarnicki⁶⁶, M. W. Slater⁵¹, J. C. Smallwood⁶¹, E. Smith⁶², K. Smith⁶⁵, M. Smith⁵⁹, A. Snoch³⁵, L. Soares Lavra⁵⁶, M. D. Sokoloff⁶³, F. J. P. Soler⁵⁷, A. Solomin^{41,52}, A. Solovev⁴¹, I. Solovyev⁴¹, R. Song¹, Y. Song⁴⁷, Y. Song⁴, Y. S. Song⁶, F. L. Souza De Almeida⁶⁶, B. Souza De Paula³, E. Spadaro Norella^{27,n}, E. Spedicato²², J. G. Speer¹⁷, E. Spiridenkov⁴¹, P. Spradlin⁵⁷, V. Sriskaran⁴⁶, F. Stagni⁴⁶, M. Stahl⁴⁶, S. Stahl⁴⁶, S. Stanislaus⁶¹, E. N. Stein⁴⁶, O. Steinkamp⁴⁸, O. Stenyakin⁴¹, H. Stevens¹⁷, D. Strelakina⁴¹, Y. Su⁷, F. Suljik⁶¹, J. Sun²⁹, L. Sun⁷¹, Y. Sun⁶⁴, P. N. Swallow⁵¹, F. Swystun⁵⁴, A. Szabelski³⁹, T. Szumlak³⁷, M. Szymanski⁴⁶, Y. Tan⁴, S. Taneja⁶⁰, M. D. Tat⁶¹, A. Terentev⁴⁸, F. Terzuoli^{32,v}, F. Teubert⁴⁶, E. Thomas⁴⁶, D. J. D. Thompson⁵¹, H. Tilquin⁵⁹, V. Tisserand¹¹, S. T'Jampens¹⁰, M. Tobin⁵, L. Tomassetti^{23,k}, G. Tonani^{27,n,46}, X. Tong⁶, D. Torres Machado², L. Toscano¹⁷, D. Y. Tou⁴, C. Trippel⁴², G. Tuci¹⁹, N. Tuning³⁵, L. H. Uecker¹⁹, A. Ukleja³⁷, D. J. Unverzagt¹⁹, E. Ursov⁴¹, A. Usachov³⁶, A. Ustyuzhanin⁴¹, U. Uwer¹⁹, V. Vagnoni²², A. Valassi⁴⁶, G. Valenti²², N. Valls Canudas⁴², H. Van Hecke⁶⁵, E. van Herwijnen⁵⁹, C. B. Van Hulse^{44,x}, R. Van Laak⁴⁷, M. van Veghel³⁵, R. Vazquez Gomez⁴³, P. Vazquez Regueiro⁴⁴, C. Vázquez Sierra⁴⁴, S. Vecchi²³, J. J. Velthuis⁵², M. Veltri^{24,w}, A. Venkateswaran⁴⁷, M. Vesterinen⁵⁴, M. Vieites Diaz⁴⁶, X. Vilasis-Cardona⁴², E. Vilella Figueras⁵⁸, A. Villa²², P. Vincent¹⁵, F. C. Volle¹³, D. vom Bruch¹², V. Vorobyev⁴¹, N. Voropaev⁴¹, K. Vos⁷⁶, G. Vouters¹⁰, C. Vrahas⁵⁶, J. Walsh³², E. J. Walton¹, G. Wan⁶, C. Wang¹⁹, G. Wang⁸, J. Wang⁶, J. Wang⁵, J. Wang⁴, J. Wang⁷¹, M. Wang²⁷, N. W. Wang⁷, R. Wang⁵², X. Wang⁶⁹, X. W. Wang⁵⁹, Y. Wang⁸, Z. Wang¹³, Z. Wang⁴, Z. Wang⁷, J. A. Ward^{54,1}, M. Waterlaet⁴⁶, N. K. Watson⁵¹, D. Websdale⁵⁹, Y. Wei⁶, B. D. C. Westhenry⁵², C. White⁵⁴, D. J. White⁶⁰, M. Whitehead⁵⁷, A. R. Wiederhold⁵⁴, D. Wiedner¹⁷, G. Wilkinson⁶¹, M. K. Wilkinson⁶³, M. Williams⁶², M. R. J. Williams⁵⁶, R. Williams⁵³, F. F. Wilson⁵⁵, W. Wislicki³⁹, M. Witek³⁸, L. Witola¹⁹, C. P. Wong⁶⁵, G. Wormser¹³, S. A. Wotton⁵³, H. Wu⁶⁶, J. Wu⁸, Y. Wu⁶, K. Wyllie⁴⁶, S. Xian⁶⁹, Z. Xiang⁵, Y. Xie⁸, A. Xu³², J. Xu⁷, L. Xu⁴, L. Xu⁴, M. Xu⁵⁴, Z. Xu¹¹, Z. Xu⁷, Z. Xu⁵, D. Yang⁴, S. Yang⁷, X. Yang⁶, Y. Yang^{26,m}, Z. Yang⁶, Z. Yang⁶⁴, V. Yeroshenko¹³, H. Yeung⁶⁰, H. Yin⁸, C. Y. Yu⁶, J. Yu⁶⁸, X. Yuan⁵, E. Zaffaroni⁴⁷, M. Zavertyaev¹⁸, M. Zdybal³⁸, M. Zeng⁴, C. Zhang⁶, D. Zhang⁸, J. Zhang⁷, L. Zhang⁴, S. Zhang⁶⁸, S. Zhang⁶, Y. Zhang⁶, Y. Z. Zhang⁴, Y. Zhao¹⁹, A. Zharkova⁴¹, A. Zhelezov¹⁹, X. Z. Zheng⁴, Y. Zheng⁷, T. Zhou⁶, X. Zhou⁸, Y. Zhou⁷, V. Zhovkovska⁵⁴, L. Z. Zhu⁷, X. Zhu⁴, X. Zhu⁸, V. Zhukov^{16,41}, J. Zhuo⁴⁵, Q. Zou^{5,7}, D. Zuliani³⁰, G. Zunica⁶⁰

¹ School of Physics and Astronomy, Monash University, Melbourne, Australia

² Centro Brasileiro de Pesquisas Físicas (CBPF), Rio de Janeiro, Brazil

³ Universidade Federal do Rio de Janeiro (UFRJ), Rio de Janeiro, Brazil

⁴ Center for High Energy Physics, Tsinghua University, Beijing, China

⁵ Institute Of High Energy Physics (IHEP), Beijing, China

⁶ School of Physics State Key Laboratory of Nuclear Physics and Technology, Peking University, Beijing, China

⁷ University of Chinese Academy of Sciences, Beijing, China

⁸ Institute of Particle Physics, Central China Normal University, Wuhan, Hubei, China

⁹ Consejo Nacional de Rectores (CONARE), San Jose, Costa Rica

¹⁰ Université Savoie Mont Blanc, CNRS, IN2P3-LAPP, Annecy, France

¹¹ Université Clermont Auvergne, CNRS/IN2P3, LPC, Clermont-Ferrand, France

¹² Aix Marseille Univ, CNRS/IN2P3, CPPM, Marseille, France

¹³ Université Paris-Saclay, CNRS/IN2P3, IJCLab, Orsay, France

¹⁴ Laboratoire Leprince-Ringuet, CNRS/IN2P3, Ecole Polytechnique, Institut Polytechnique de Paris, Palaiseau, France

¹⁵ LPNHE, Sorbonne Université, Paris Diderot Sorbonne Paris Cité, CNRS/IN2P3, Paris, France

¹⁶ I. Physikalisches Institut, RWTH Aachen University, Aachen, Germany

¹⁷ Fakultät Physik, Technische Universität Dortmund, Dortmund, Germany

¹⁸ Max-Planck-Institut für Kernphysik (MPIK), Heidelberg, Germany

¹⁹ Physikalisches Institut, Ruprecht-Karls-Universität Heidelberg, Heidelberg, Germany

²⁰ School of Physics, University College Dublin, Dublin, Ireland

²¹ INFN Sezione di Bari, Bari, Italy

²² INFN Sezione di Bologna, Bologna, Italy

²³ INFN Sezione di Ferrara, Ferrara, Italy

- 24 INFN Sezione di Firenze, Firenze, Italy
- 25 INFN Laboratori Nazionali di Frascati, Frascati, Italy
- 26 INFN Sezione di Genova, Genoa, Italy
- 27 INFN Sezione di Milano, Milan, Italy
- 28 INFN Sezione di Milano-Bicocca, Milan, Italy
- 29 INFN Sezione di Cagliari, Monserrato, Italy
- 30 Università degli Studi di Padova, Università e INFN, Padua, Italy
- 31 INFN Sezione di Perugia, Perugia, Italy
- 32 INFN Sezione di Pisa, Pisa, Italy
- 33 INFN Sezione di Roma La Sapienza, Rome, Italy
- 34 INFN Sezione di Roma Tor Vergata, Rome, Italy
- 35 Nikhef National Institute for Subatomic Physics, Amsterdam, The Netherlands
- 36 Nikhef National Institute for Subatomic Physics and VU University Amsterdam, Amsterdam, The Netherlands
- 37 AGH-University of Science and Technology, Faculty of Physics and Applied Computer Science, Kraków, Poland
- 38 Henryk Niewodniczanski Institute of Nuclear Physics Polish Academy of Sciences, Kraków, Poland
- 39 National Center for Nuclear Research (NCBJ), Warsaw, Poland
- 40 Horia Hulubei National Institute of Physics and Nuclear Engineering, Bucharest-Magurele, Romania
- 41 Affiliated with an institute covered by a cooperation agreement with CERN, Geneva, Switzerland
- 42 DS4DS, La Salle, Universitat Ramon Llull, Barcelona, Spain
- 43 ICCUB, Universitat de Barcelona, Barcelona, Spain
- 44 Instituto Galego de Física de Altas Enerxías (IGFAE), Universidade de Santiago de Compostela, Santiago de Compostela, Spain
- 45 Instituto de Física Corpuscular, Centro Mixto Universidad de Valencia-CSIC, Valencia, Spain
- 46 European Organization for Nuclear Research (CERN), Geneva, Switzerland
- 47 Institute of Physics, Ecole Polytechnique Fédérale de Lausanne (EPFL), Lausanne, Switzerland
- 48 Physik-Institut, Universität Zürich, Zurich, Switzerland
- 49 NSC Kharkiv Institute of Physics and Technology (NSC KIPT), Kharkiv, Ukraine
- 50 Institute for Nuclear Research of the National Academy of Sciences (KINR), Kyiv, Ukraine
- 51 University of Birmingham, Birmingham, UK
- 52 H.H. Wills Physics Laboratory, University of Bristol, Bristol, UK
- 53 Cavendish Laboratory, University of Cambridge, Cambridge, UK
- 54 Department of Physics, University of Warwick, Coventry, UK
- 55 STFC Rutherford Appleton Laboratory, Didcot, UK
- 56 School of Physics and Astronomy, University of Edinburgh, Edinburgh, UK
- 57 School of Physics and Astronomy, University of Glasgow, Glasgow, UK
- 58 Oliver Lodge Laboratory, University of Liverpool, Liverpool, UK
- 59 Imperial College London, London, UK
- 60 Department of Physics and Astronomy, University of Manchester, Manchester, UK
- 61 Department of Physics, University of Oxford, Oxford, UK
- 62 Massachusetts Institute of Technology, Cambridge, MA, USA
- 63 University of Cincinnati, Cincinnati, OH, USA
- 64 University of Maryland, College Park, MD, USA
- 65 Los Alamos National Laboratory (LANL), Los Alamos, NM, USA
- 66 Syracuse University, Syracuse, NY, USA
- 67 Pontifícia Universidade Católica do Rio de Janeiro (PUC-Rio), Rio de Janeiro, Brazil, associated to ³
- 68 School of Physics and Electronics, Hunan University, Changsha City, China, associated to ⁸
- 69 Guangdong Provincial Key Laboratory of Nuclear Science, Guangdong-Hong Kong Joint Laboratory of Quantum Matter, Institute of Quantum Matter, South China Normal University, Guangzhou, China, associated to ⁴
- 70 Lanzhou University, Lanzhou, China, associated to ⁵
- 71 School of Physics and Technology, Wuhan University, Wuhan, China, associated to ⁴
- 72 Departamento de Física, Universidad Nacional de Colombia, Bogota, Colombia, associated to ¹⁵
- 73 Universität Bonn-Helmholtz-Institut für Strahlen und Kernphysik, Bonn, Germany, associated to ¹⁹
- 74 Eotvos Lorand University, Budapest, Hungary, associated to ⁴⁶

- ⁷⁵ Van Swinderen Institute, University of Groningen, Groningen, The Netherlands, associated to ³⁵
- ⁷⁶ Universiteit Maastricht, Maastricht, The Netherlands, associated to ³⁵
- ⁷⁷ Tadeusz Kosciuszko Cracow University of Technology, Kraków, Poland, associated to ³⁸
- ⁷⁸ Department of Physics and Astronomy, Uppsala University, Uppsala, Sweden, associated to ⁵⁷
- ⁷⁹ University of Michigan, Ann Arbor, MI, USA, associated to ⁶⁶
- ⁸⁰ Departement de Physique Nucleaire (SPhN), Gif-Sur-Yvette, France
- ^a Universidade de Brasília, Brasília, Brazil
- ^b Centro Federal de Educação Tecnológica Celso Suckow da Fonseca, Rio De Janeiro, Brazil
- ^c Hangzhou Institute for Advanced Study, UCAS, Hangzhou, China
- ^d School of Physics and Electronics, Henan University, Kaifeng, China
- ^e LIP6, Sorbonne Universite, Paris, France
- ^f Excellence Cluster ORIGINS, Munich, Germany
- ^g Universidad Nacional Autónoma de Honduras, Tegucigalpa, Honduras
- ^h Università di Bari, Bari, Italy
- ⁱ Università di Bologna, Bologna, Italy
- ^j Università di Cagliari, Cagliari, Italy
- ^k Università di Ferrara, Ferrara, Italy
- ^l Università di Firenze, Firenze, Italy
- ^m Università di Genova, Genoa, Italy
- ⁿ Università degli Studi di Milano, Milan, Italy
- ^o Università di Milano Bicocca, Milan, Italy
- ^p Università di Padova, Padua, Italy
- ^q Università di Perugia, Perugia, Italy
- ^r Scuola Normale Superiore, Pisa, Italy
- ^s Università di Pisa, Pisa, Italy
- ^t Università della Basilicata, Potenza, Italy
- ^u Università di Roma Tor Vergata, Rome, Italy
- ^v Università di Siena, Siena, Italy
- ^w Università di Urbino, Urbino, Italy
- ^x Universidad de Alcalá, Alcalá de Henares, Spain
- ^y Universidade da Coruña, Coruna, Spain
- ^z Department of Physics/Division of Particle Physics, Lund, Sweden
- *Deceased